

Contents lists available at ScienceDirect

## Journal of Sound and Vibration

journal homepage: www.elsevier.com/locate/jsvi





# Stochastic thermal modal characteristics of a plate with free boundary conditions induced by a random heating position based on a thermally coupled model

Yu-Jia Hu<sup>a</sup>, Lei Hu<sup>a</sup>, Weidong Zhu<sup>b,\*</sup>, Haolin Li<sup>a</sup>

- <sup>a</sup> School of Mechanical Engineering, University of Shanghai for Science and Technology, Shanghai 200093, China
- b Department of Mechanical Engineering, University of Maryland, Baltimore County, 1000 Hilltop Circle, Baltimore, MD 21250, USA

### ARTICLE INFO

#### Keywords:

Thermally coupled dynamic model Stochastic thermal modal analysis Dynamic characteristics at high temperature Small sample estimation

### ABSTRACT

Temperature has significant effects on thermal modal characteristics of a structure; especially, its distribution uncertainty makes thermal modal characteristics to be more complicated. Such uncertainty also makes definitely predicted results greatly deviate from thermal modal experimental results at high temperature, and even their change trends with temperature would be different. In this work, stochastic thermal modal characteristics of a plate with free boundary conditions induced by a random heating position are studied based on a thermally coupled model. Temperature field distributions of the plate under two-parameter Gaussian heating sources are first obtained. A thermally coupled dynamic model of the plate is then established based on a thermally coupled constitutive relation theory, and its modal parameters are obtained by a differential quadrature method. A statistical analysis method with a small sample based on an improved Bootstrap method and folded normal distribution is proposed to study stochastic thermal modal characteristics of the plate induced by a random heating position, which includes probability density functions of natural frequencies and their confidence intervals. Relevant research will be of great significance to reliability evaluation of thermodynamic experimental results, and error analysis between experimental and theoretical results.

### 1. Introduction

Temperature causes changes in mechanical properties of materials in a high-temperature environment and generates thermal stresses in structures due to such factors as changes in constraints and nonuniform heating on the structures, thereby possibly impacting stiffnesses and vibration characteristics of the structures. Related theoretical research focuses on variation mechanisms and experiments of thermal dynamic characteristics of a structure at high temperature, such as beams or laminated beams [1,2], composite plates or stiffened plates, and so on with different boundary conditions [3–5]. The main research aspects include thermal dynamic models of a structure [1,3], variations of modal parameters of a structure with temperature [6–8], transient dynamic characteristics of a structure [4], effects of a temperature field [5,9], and so on. It can be found from theoretical and experimental results that temperature and its distribution have significant effects on dynamic characteristics, such as natural frequencies and mode shapes, of a structure. A jump phenomenon in mode shapes [4,8] and the non-monotonical behavior of natural frequencies [10–12] were found in dynamic experiments.

<sup>\*</sup> Corresponding author.

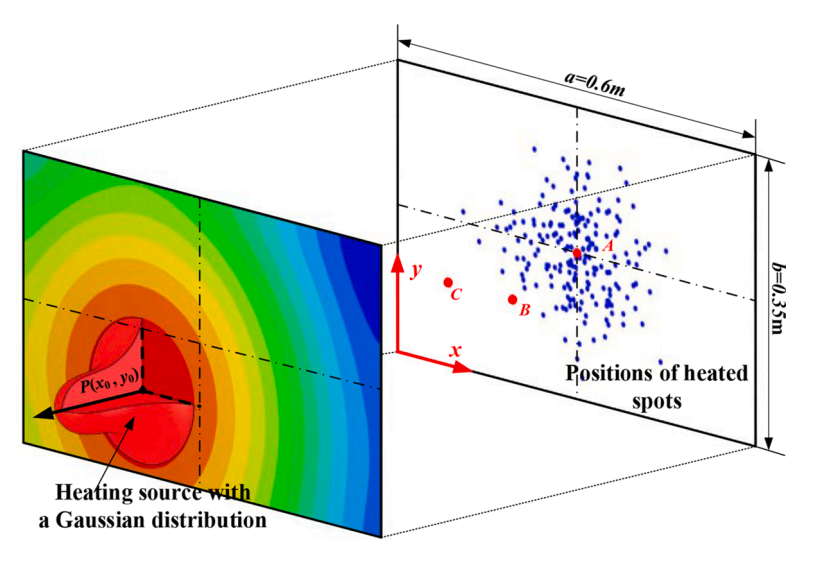


Fig. 1. Physical model of a titanium plate with a Gaussian heating source and distribution of heated spots

Although there is rich related theoretical research on thermal dynamic characteristics of a structure, there are two shortcomings: first, uncoupled constitutive relations by considering effects of temperature on mechanical properties of materials are used in theotetical and numerical analyses. Based on the theory of a thermally stressed plate and uncoupled constitutive relations where material parameters are constant, which do not change with temperature, thermal modal characteristics of a plate with free boundary conditions under non-uniform temperature fields were studied and some phenomena were found [13,14]. However, natural frequencies of a plate with free boundary conditions under a uniform temperature field obtained by the above mentioned uncoupled model will almost not change with temperature because thermal stresses under the uniform temperature field of the plate are constant. Changes of natural frequencies of the plate obtained by the above mentioned uncoupled model with temperature is mainly caused by gradients of the temperature field. Obviously, it is inappropriate to ignore effects of thermal coupling in constitutive relations on thermal modal characteristics of the plate. In order to consider the effect of temperature on a material, equivalent Young's moduli and Possion's ratios under different high temperatures, which are obtained by material experiments, are used in thermal dynamic models of structures. Due to limited experimental results of mechanical properties of materials at different high temperatures, a linear interpolation of mechanical properties is often used to obtain mechanical properties of materials in the full temperature field, which lacks a rigorous theoretical basis. Further thermal modal theoretical research was to introduce nonlinear temperature influence terms into constitutive relations, which established a thermal modal analysis model of a structure [15]. However, direct introduction of nonlinear temperature influence terms into constitutive relations would make constitutive relations to not satisfy tensor characteristics on a theoretical basis. Therefore, it is important to study dynamic characteristics of a structure based on coupled constitutive relations. Second, predicted results, such as natural frequencies and mode shapes, of a structure deviate greatly from thermal modal experimental results at high temperature, and even their change trends with temperature would be different [12]. With the development of the aerospace industry, the study of thermal modal experiments at high tempertature was fast developed by contact and non-contact experimental methods [9,12,16,17]. The experimental reliability at high temperature is greatly increased. Many dynamic experimental phenomena at high temperature were found, such as some disappearing modes with an increasing rate of temperature rise [6], and occurrences of the non-monotonical behavior of natural frequencies and interchange of mode shapes [8,10-12]. However, predicted results are always not consistent with thermal dynamic experiments due to the fact that temperature and its distribution have significant effects on thermal modal characteristics of a structure. It is difficult to accurately control the temperature field in thermal dynamic experiments. Different experimental uncertainties, such as uncertainties of the heating position and environment, greatly affect thermal modal characteristics of a structure. Such uncertainties are more obvious in thermal dynamic experiments under working conditions of a structure. Recently, some researchers realized that it was not suitable to use a definite theory to analyze thermal modal characteristics of a structure. Histograms of natural frequencies were obtained to describe distribution characteristics of a structure at high temperature, which were closer to those from thermal modal experiments [11]. However, how to carry out research on statistical characteristics of thermal modes of a structure under a small sample, how to obtain more useful information from distribution of natural frequencies, and how to obtain confidence intervals of predicted results are still unanswered.

The remaining part of this paper is organized as follows. In order to accurately predict thermal modal characteristics of a plate and evaluate statistical characteristics of modal parameters of the plate at high temperature, temperature field distributions of the plate under Gaussian heat sources with different heating positions at different heating times are obtained in Sec. 2 by a finite element method (FEM), and a modified Gaussian function is used there to describe temperature fields to reduce violent oscillations of numerical results caused by direct use of discrete temperatures for their derivative calculations and to improve the calculation accuracy. A strict thermally coupled constitutive relation theory is used in Sec. 3 to establish a thermally coupled dynamic model of the plate under a non-uniform temperature field, and its natural frequencies are obtained in Sec. 4 by a differential quadrature method (DQM). A

**Table 1**Simulation parameters

Parameter	Value		
Density	4620 kg/m <sup>3</sup>		
Isotropic Thermal Conductivity	21.9 W/m•°C		
Specific Heat	522 J/(kg• °C)		
Element Size	0.01 m		
Room Temperature	20 °C		
Film Coefficient	5 W/m <sup>2</sup> •°C		
Emissivity	0.65		

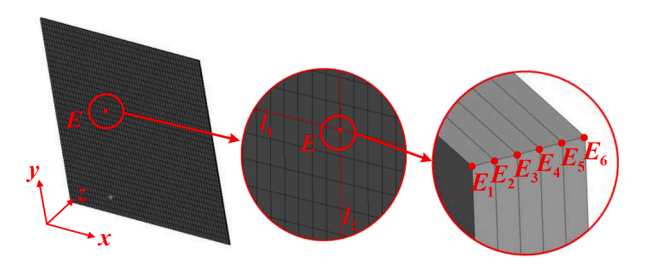


Fig. 2. Meshed model and its section along lines  $l_1$  and  $l_2$ 

**Table 2** Temperatures at the point E in the thickness direction of the plate with different heated spots A, B and C

Heating Position	Node $E_1$ /°C	Node E <sub>6</sub> ∕°C	Difference /°C
A	463.74	464.96	1.22
В	459.83	461.07	1.24
С	102.02	102.98	0.96

statistical analysis method with a small sample is used in Sec. 5 to study statistical properties of the plate induced by a random heating position, which includes probability density distributions (PDFs) of natural frequencies and their confidences and confidence intervals. Finally, some conclusions are presented in Sec. 6.

### 2. Temperature Field Distributions of the Plate under Gaussian Heat Sources at Different Heating Times

Temperature and its distribution highly affect dynamic characteristics of a structure, which makes thermal dynamic analysis more complex. The uncertainty of the heating position is one of the most important factors that affect the uncertainty of the temperature field of the structure. In order to describe influence of the heating position on thermal modal characteristics of a titanium plate with its size being  $a \times b \times c$ , as shown in Fig. 1, it can be assumed that the Gaussian heating source acts at the heated spot  $P(x_0, y_0)$  of the plate. By considering the uncertainty of the heating position, two parameters  $\alpha$  and  $\beta$  are introduced, which satisfy  $\alpha$ ,  $\beta \sim N(0, 0.05^2)$ . By letting  $x_0 = a/2 + \alpha$  and  $y_0 = b/2 + \beta$ , distribution of the heat flux  $\tilde{q}$  over the heated spot is approximately described by the Gaussian function [18.19]

$$\widetilde{q} = Q \exp\left(-\left((x - x_0)^2 + (y - y_0)^2\right) / \left(r/\sqrt{3}\right)^2\right)$$
 (1)

where Q is the maximum heat flux and r=0.4 m. In order to simulate the uncertainty of the heating position, 200 random samples of  $\alpha$  and  $\beta$  are used in this work; detailed heated spots are shown in Fig. 1 and listed in Table A1 in Appendix A. It can be seen that the density of samples is gradually sparse from the geometrical center of the titanium plate to the edge. Unless otherwise specified, the size of the titanium plate is  $0.6 \text{ m} \times 0.35 \text{ m} \times 0.002 \text{ m}, Q=3\times 10^4 \text{ W/m}^2$ , and other simulation parameters are given in Table 1. It is noted that three heated spots with positions A(0.3 m, 0.175 m), B(0.2 m, 0.1 m) and C(0.1 m, 0.1 m) are used in this work for convenience of explanation. The commercial software ANSYS is used to analyze transient temperature distributions of the titanium plate under different Gaussian heating sources at different heating times, and the corresponding analysis process with use of ANSYS is shown in Ref. [19].

The meshed model of the titanium plate is shown in Fig. 2. Table 2 shows temperatures at the point E(0.2 m, 0.2 m) along the thickness of the plate at the heating time t=250 s when heated spots are A, B and C. It can be seen that the maximum temperature difference along the thickness is not larger than 1.3 °C, as shown in Table 2. Therefore, the average temperature in the thickness direction is used in the following analyses instead of temperature distribution in the thickness direction.

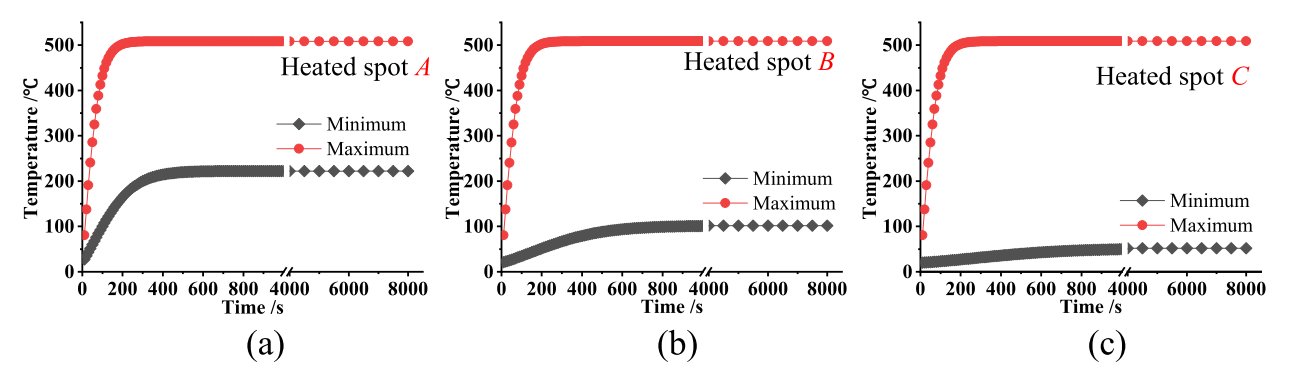


Fig. 3. Temperature changes with the heating time at different heated spots, where (a)-(c) correspond to heated spots A, B and C, respectively

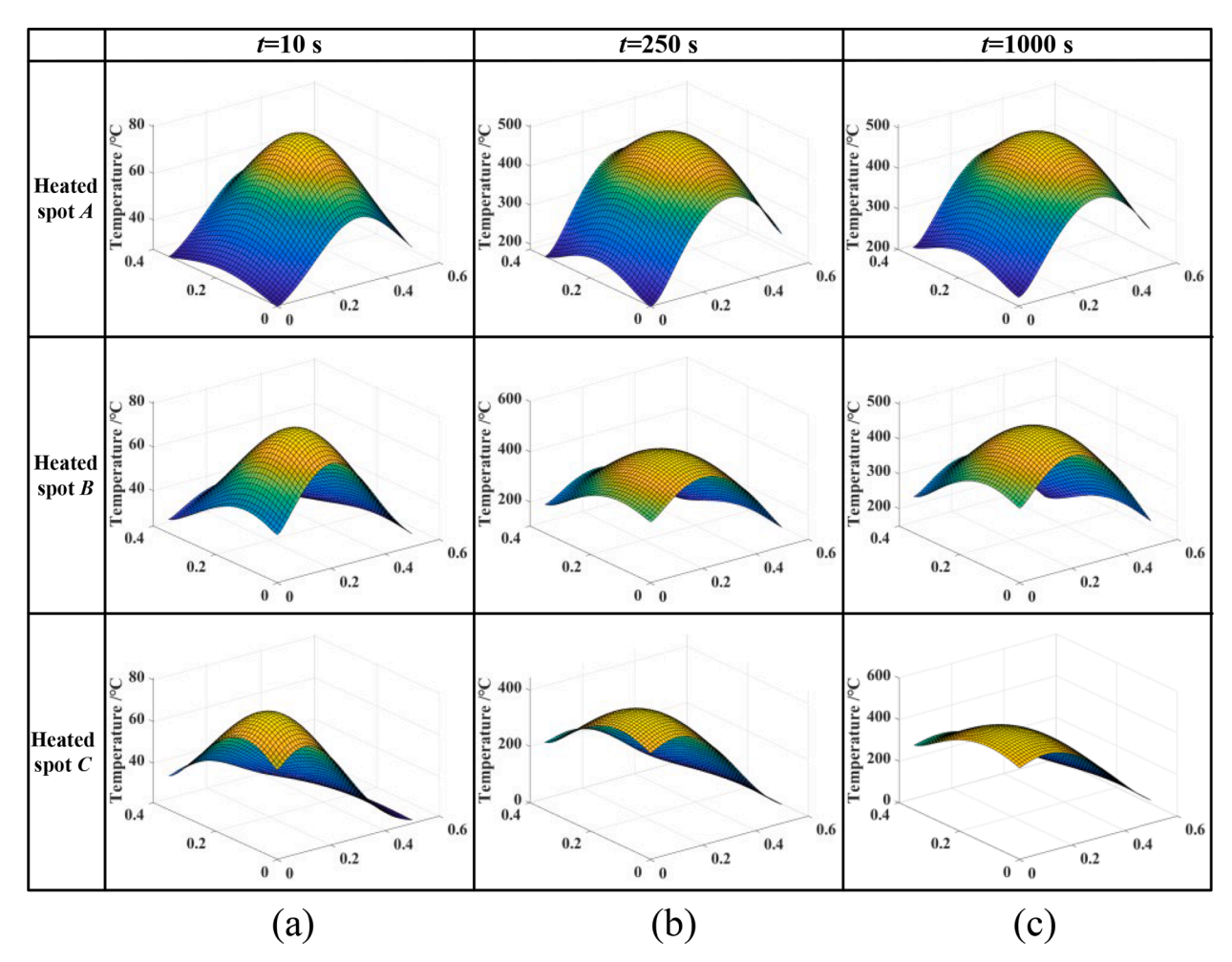


Fig. 4. Temperature field distributions of the titanium plate with different heated spots A, B and C at different heating times, where (a)-(c) correspond to heating times t = 15 s, t = 250 s and t = 10000 s, respectively

The highest and lowest temperatures on the titanium plate with different heated spots A, B and C as a function of the heating time are shown in Fig. 3. It can be seen that the highest and lowest temperatures take 250 s and 1000 s to reach steady state, respectively. Temperature field distributions of the titanium plate at heating times  $t=15\,$  s,  $t=250\,$  s and  $t=1000\,$  s are shown in Fig. 4. In order to reduce violent oscillations of numerical results caused by direct use of discrete temperatures for their derivative calculations and to obtain more accurate derivatives of the non-uniform temperature field in the following analyses, a modified Gaussian function is used to describe the dimensionless temperature field:

**Table 3** Fitted values of  $T_O$ ,  $R_O$ ,  $d_O$  and corresponding coefficients of determination  $R^2$  with different heated spots and heating times

Heated spot	Heating time /s	$T_Q$	$R_Q$ /m	$d_Q$	$R^2$
A	10	3.024141	0.231107	0.020630	0.9996
	30	8.621528	0.233605	0.080714	0.9990
	50	13.20158	0.240462	0.067387	0.9981
	250	24.72248	0.321820	2.05E-15	0.9947
	1000	22.36368	0.327503	2.185605	0.9970
	8000	22.36198	0.327489	2.187304	0.9969
В	10	3.044806	0.232356	9.68E-16	0.9998
	30	8.711131	0.234998	1.25E-15	0.9993
	50	11.95891	0.245694	4.65E-16	0.9982
	250	24.89881	0.301823	1.04E-15	0.9912
	1000	24.73871	0.338022	2.81E-16	0.9959
	8000	24.72797	0.338419	2.63E-15	0.9960
С	10	3.049625	0.232012	3.00E-16	0.9998
	30	8.737664	0.234250	4.59E-16	0.9996
	50	13.64971	0.237915	2.04E-17	0.9993
	250	21.84155	0.287503	1.06E-15	0.9962
	1000	25.05201	0.324783	9.59E-16	0.9959
	8000	24.97439	0.327811	1.02E-15	0.9967

$$T^* = T_Q \exp\left(-3(x - x_0)^2 + (y - y_0)^2 / R_Q^2\right) + d_Q \tag{2}$$

where  $d_Q$  is an additional boundary correction term that considers influence of boundaries;  $T^* = \Delta T/T_0 = (T-T_0)/T_0$  is a dimensionless temperature, in which T and  $T_0 = 20$  °C are the present temperature and room temperature, respectively; and  $T_Q$ ,  $R_Q$ ,  $d_Q$  are variables that need to be fitted by numerical results of a temperature field. Table 3 lists fitted values of  $T_Q$ ,  $T_Q$ ,  $T_Q$ , and corresponding coefficients of determination  $T_Q$  with different heated spots and heating times. One can find that the modified Gaussian function used in this work has a good precision that can be used to describe temperature distributions of the titanium plate under Gaussian heating sources. Fitted values of temperature fields of 200 random Gaussian heating sources are given in Table A1 in Appendix A.

### 3. Coupled Thermodynamic Model of the Plate

### 3.1. Thermally Coupled Constitutive Relations

The key to establish a thermal dynamic model of a structure is to use thermally coupled constitutive relations to describe a thermomechanical coupled characteristic of a material. For a simple material, the state function of a particle of the material is independent of motion and temperature histories, which is only determined by the current state. In general, coupled constitutive relations of a material can be obtained by a strain energy function as functions of a dimensionless temperature  $T^*$  and strain invariants  $I_1$ ,  $I_2$  and  $I_3$ . When the strain tensor  $|r_{ij}| \ll 1$ , where i,j=1,2,3, a strain energy function  $\Phi$  can be expressed as a power series. It is further noted that effects of the strain tensor over the third order and those of products of the dimensionless temperature over the fourth order are neglected. The strain energy function can be simplified as [20,21]

$$\Phi = a_1 + a_2 T^* + a_3 T^{*2} + a_4 T^{*3} + a_5 T^{*4} + a_6 I_1 + a_7 I_1 T^* + a_8 I_1 T^{*2} 
+ a_9 I_1 T^{*3} + a_{10} I_1^2 + a_{11} I_1^2 T^* + a_{12} I_1^2 T^{*2} + a_{13} I_1^3 + a_{14} I_1^3 T^* + a_{15} I_2 
+ a_{16} I_2 T^* + a_{17} I_2 T^{*2} + a_{18} I_1 I_2 + a_{19} I_1 I_2 T^* + a_{20} I_3 + a_{21} I_3 T^*$$
(3)

where  $a_0, a_1, \dots, a_{21}$  are material constants of the strain energy function. Stress-strain constitutive equations can be derived as

$$\sigma_{ij} = \frac{\partial \Phi}{\partial \gamma_{ij}} = \frac{\partial \Phi}{\partial I_1} \frac{\partial I_1}{\partial \gamma_{ij}} + \frac{\partial \Phi}{\partial I_2} \frac{\partial I_2}{\partial \gamma_{ij}} + \frac{\partial \Phi}{\partial I_3} \frac{\partial I_3}{\partial \gamma_{ij}} \tag{4}$$

where  $\frac{\partial I_1}{\partial \gamma_{ij}} = \delta_{ij}$ ,  $\frac{\partial I_2}{\partial \gamma_{ij}} = I_1 \delta_{ij} - \gamma_{ij}$  and  $\frac{\partial I_3}{\partial \gamma_{ij}} = I_2 \delta_{ij} - I_1 \gamma_{ij} + \gamma_{jk} \gamma_{ki}$ . By neglecting high-order strains, thermally coupled stress-strain constitutive equations can be obtained [21]:

$$\sigma_{11} = \chi(T^*)T^* + \psi(T^*)\gamma_{11} + [\psi(T^*) + \xi(T^*)]\gamma_{22}$$
(5a)

$$\sigma_{22} = \chi(T^*)T^* + [\psi(T^*) + \xi(T^*)]\gamma_{11} + \psi(T^*)\gamma_{22}$$
(5b)

$$\sigma_{12} = -\xi(T^*)\gamma_{12}$$
 (5c)

where  $\sigma_{11}, \sigma_{22}, \sigma_{12}$  and  $\gamma_{11}, \gamma_{22}, \gamma_{12}$  are stress components and strain components, respectively, and  $\xi(T^*) = a_{15} + a_{16}T^* + a_{17}T^{*2}, \psi(T^*)$ 

**Table 4**Equivalent Young's moduli, Poisson's ratios and coefficients of thermal expansion at different temperatures

Temp.	$E(T^*)$ /GPa	$\nu(T^*)$	$\alpha(T^*) / \times 10^{-6}  {}^{\circ}\mathrm{C}^{-1}$
20°C	113.14	0.263	_
200°C	98.77	0.299	7.59
400°C	71.98	0.322	9.475
600°C	24.76	0.347	11.75

 $=2(a_{10}+a_{11}T^*+a_{12}T^{*2})$  and  $\chi(T^*)=a_7+a_8T^*+a_9T^{*2}$  are functions of the dimensionless temperature. In order to facilitate applications, equivalent Young's moduli  $E(T^*)$ , Poisson's ratios  $v(T^*)$  and coefficients of thermal expansion  $\alpha(T^*)$  at different dimensionless temperatures are introduced. Functions of the dimensionless temperature  $\xi(T^*)$ ,  $\psi(T^*)$  and  $\chi(T^*)$  can be described by equivalent parameters  $E(T^*)$ ,  $v(T^*)$  and  $\alpha(T^*)$  at different dimensionless temperatures [21]:

$$\xi(T^*) = a_{15} + a_{16}T^* + a_{17}T^{*2} = -\frac{E(T^*)}{v(T^*) + 1}$$
(6a)

$$\psi(T^*) = 2(a_{10} + a_{11}T^* + a_{12}T^{*2}) = \frac{E(T^*)}{1 - v^2(T^*)}$$
(6b)

$$\chi(T^*) = a_7 + a_8 T^* + a_9 T^{*2} = \frac{T_0 E(T^*) \alpha(T^*)}{\nu(T^*) - 1}$$
(6c)

Material constants  $a_i$ , where  $i=7,8,\cdots,12,15,16,17$  can be fitted by the least squares method when equivalent material parameters  $E(T^*)$ ,  $v(T^*)$  and  $\alpha(T^*)$  at different dimensionless temperatures are obtained by mechanical property experiments at high temperature. By use of a laser engraving technology and three-dimensional digital image correlation proposed in Ref. [22], Young's moduli, Poisson's ratios, and coefficients of thermal expansion of the titanium plate at 20°C, 200°C, 400°C and 600°C are listed in Table 4.

By use of Eqs. 6(a)-(c), expressions of functions of equivalent material parameters  $\xi(T^*)$ ,  $\psi(T^*)$  and  $\chi(T^*)$  of the titanium plate are

$$\xi(T^*) = a_{15} + a_{16}T^* + a_{17}T^{*2} = -8.309 \times 10^{10} + 1.318 \times 10^8 T^* + 7.24 \times 10^7 T^{*2}$$
(7a)

$$\psi(T^*) = 2(a_{10} + a_{11}T^* + a_{12}T^{*2}) = 2(5.693 \times 10^{10} + 2.3 \times 10^8 T^* - 5.9 \times 10^7 T^{*2})$$
(7b)

$$\gamma(T^*) = a_7 + a_8 T^* + a_9 T^{*2} = 2.324 \times 10^8 - 6.415 \times 10^7 T^* + 1.618 \times 10^6 T^{*2}$$
 (7c)

## 3.2. Coupled Thermal Dynamic Governing Equation of the Plate under a Non-uniform Temperature Field

Under the assumption of small deformation, geometrical relations can be given by

$$\varepsilon_x = -\frac{\partial^2 w}{\partial x^2} z, \ \varepsilon_y = -\frac{\partial^2 w}{\partial y^2} z, \ \gamma_{xy} = -2 \frac{\partial^2 w}{\partial y \partial y} z \tag{8}$$

where  $\varepsilon_x$ ,  $\varepsilon_y$  and  $\gamma_{xy}$  are normal strains in x and y directions and the shear strain, respectively, and w = w(x, y, t) is the deflection of the plate. Coupled thermal dynamic governing equations can be derived via Hamilton's principle

$$\delta \int_{t_0}^t (K - H) \mathrm{d}t + \int_{t_0}^t \delta R \mathrm{d}t = 0 \tag{9}$$

where variation of the potential energy  $\delta H$ , variation of the kinetic energy  $\delta K$ , and the virtual work  $\delta R$  due to the mechanical load q = q(x, y, t) are

$$\delta H = \int \int \int_{V} (\sigma_{x} \delta \varepsilon_{x} + \sigma_{y} \delta \varepsilon_{y} + \tau_{xy} \delta \gamma_{xy}) dV$$
 (10)

$$\delta K = \int \int \int_{V} \rho \dot{w} \delta \dot{w} dV \tag{11}$$

$$\delta R = \iint_{S} q \delta w ds \tag{12}$$

respectively, in which  $\dot{w}$  is the vibration velocity, and  $\rho$  is the density of the material. By keeping Eqs. (5) and (8) in mind, substituting  $\delta H$ ,  $\delta K$  and  $\delta R$  into Eq. (9), and letting  $w(x,y,t) = \bar{w}(x,y)e^{i\omega t}$ , where i is the imaginary unit and  $\omega$  is the excitation frequency, the coupled thermal dynamic governing equation of the titanium plate under a non-uniform temperature field can be obtained, with detailed

**Table 5**Boundary conditions of the titanium plate

Boundary condition	Mathematical equations
fixed end	$ \bar{w} _{x=0} = 0, \frac{\partial \bar{w}}{\partial x} _{x=0} = 0$
hinged end	$\bar{w} _{x=0} = 0, \xi(T^*(x,y)) \frac{\partial^2 \bar{w}}{\partial y^2} _{x=0} + \psi(T^*(x,y)) \frac{\partial^2 \bar{w}}{\partial y^2} _{x=0} + \psi(T^*(x,y)) \frac{\partial^2 \bar{w}}{\partial x^2} _{x=0} = 0$
free end	$\begin{split} &\left(\frac{\partial \underline{\xi}(T^{*}(x,y))}{\partial x} + \frac{\partial \psi(T^{*}(x,y))}{\partial x}\right)\frac{\partial^{2} \bar{w}}{\partial y^{2}}\big _{x=0} - \left(\frac{\partial \underline{\xi}(T^{*}(x,y))}{\partial y} + \frac{\partial \xi(T^{*}(x,y))}{\partial x}\right) \\ &\frac{\partial^{2} \bar{w}}{\partial x \partial y}\big _{x=0} + \psi(T^{*}(x,y))\frac{\partial^{3} \bar{w}}{\partial x \partial y^{2}}\big _{x=0} + \frac{\partial \psi(T^{*}(x,y))}{\partial x}\frac{\partial^{2} \bar{w}}{\partial x^{2}}\big _{x=0} - \underline{\xi}(T^{*}(x,y)) \end{split}$
	$\frac{\partial x \partial y}{\partial x^2 \partial y}\Big _{x=0} + \psi(T(x,y)) \frac{\partial^3 \bar{w}}{\partial x \partial y^2}\Big _{x=0} + \frac{\partial^3 \bar{w}}{\partial x^2 \partial y}\Big _{x=0} + \psi(T^*(x,y)) \frac{\partial^3 \bar{w}}{\partial x^3}\Big _{x=0} = 0, \xi(T^*(x,y)) \frac{\partial^2 \bar{w}}{\partial x \partial y}\Big _{x=0,y=0} = 0$

derivation given in Appendix B:

$$D[\psi(T^{*}(x,y))\left(\frac{\partial^{4}\bar{w}}{\partial x^{4}}+2\frac{\partial^{4}\bar{w}}{\partial x^{2}\partial y^{2}}+\frac{\partial^{4}\bar{w}}{\partial y^{4}}\right)+\left(\frac{\partial^{2}(\psi(T^{*}(x,y)+\xi(T^{*}(x,y))))}{\partial y^{2}}\right)$$

$$+\frac{\partial^{2}\psi(T^{*}(x,y))}{\partial x^{2}})\frac{\partial^{2}\bar{w}}{\partial x^{2}}+\left(\frac{\partial^{2}\psi(T^{*}(x,y))}{\partial y^{2}}+\frac{\partial^{2}(\psi(T^{*}(x,y)+\xi(T^{*}(x,y))))}{\partial x^{2}}\right)\frac{\partial^{2}\bar{w}}{\partial y^{2}}$$

$$-2\frac{\partial^{2}\xi(T^{*}(x,y))}{\partial x\partial y}\frac{\partial^{2}\bar{w}}{\partial x\partial y}+2\frac{\partial\psi(T^{*}(x,y))}{\partial x}\frac{\partial^{3}\bar{w}}{\partial x^{3}}+2\frac{\partial\psi(T^{*}(x,y))}{\partial y}\frac{\partial^{3}\bar{w}}{\partial y^{3}}$$

$$+2\frac{\partial\psi(T^{*}(x,y))}{\partial x}\frac{\partial^{3}\bar{w}}{\partial y^{2}\partial x}+2\frac{\partial\psi(T^{*}(x,y))}{\partial y}\frac{\partial^{3}\bar{w}}{\partial x^{2}\partial y}]-\rho\hbar\omega^{2}\bar{w}=0$$

$$(13)$$

where  $D = h^3/12$ . Corresponding boundary conditions of the titanium plate can also be obtained, which are listed in Table 5.

It is noted that effects of thermal coupling on the plate generally include two parts: the thermal mechanical coupled effect in constitutive relations, and the thermal mechanical coupled effect in the heat equation. The thermal mechanical coupled effect in constitutive relations is considered in the present work. Strictly speaking, the thermally coupled model should consider the thermal mechanical coupled effect in the heat equation. However, one can find that changes of temperature with time under Gaussian heating sources are slow when the change of the temperature field is not particularly violent. Therefore, similar to the treatment in Refs. [13, 14], such a coupled effect is neglected in the present work.

### 3.3. Simulation Method

The DQM is employed to numerically solve coupled thermal dynamic governing equations in Eq. (13), with boundary conditions listed in Table. 5. The fundamental idea behind the DQM is to approximate an unknown function and its derivatives at any discrete point as linear weighted sums of its values at all discrete points chosen in the solution domain [23]. By considering a function  $\bar{w}(x,y)$  in a domain  $\{(x,y) \in (0 \le x \le a, 0 \le y \le b)\}$ , its rth derivative with respect to x and y are approximated by [23]

$$\frac{\partial^r \bar{w}}{\partial x^r}|_{x=x_i} = \sum_{k=1}^{N_x} A_{ik}^{(r)} \bar{w}_{kj}, \quad \frac{\partial^s \bar{w}}{\partial y^s}|_{y=y_j} = \sum_{l=1}^{N_y} B_{jl}^{(s)} \bar{w}_{il}$$
(14a)

The associated (r+s)th derivative of  $\bar{w}(x,y)$  with respect to x and y is

$$\frac{\partial^{(r+s)}\bar{w}}{\partial x^r\partial y^s}\Big|_{x_i,y_j} = \frac{\partial^r}{\partial x^r} \left(\frac{\partial^s \bar{w}}{\partial y^s}\right)\Big|_{x_i,y_j} = \sum_{k=1}^{N_z} A_{ik}^{(r)} \sum_{l=1}^{N_y} B_{jl}^{(s)} \bar{w}_{kl}$$
(14b)

where  $i=1,2,\cdots,N_x$  and  $j=1,2,\cdots,N_y$ , in which  $N_x$  and  $N_y$  are grid points in x and y directions on the plate;  $\bar{w}_{ij}=\bar{w}(x_j,y_j)$ ; and  $A_{ik}^{(r)}$  and  $B_{jl}^{(r)}$  are weighting coefficients dependent on coordinates of discrete points only, which can be calculated through a recursive formula. It should be mentioned that zeros of the Chebyshev–Lobatto polynomial are taken as coordinates of grid points here due to its excellent convergence. The discretized governing equation can be obtained as

Table 6 Convergence of the numerical method of natural frequencies with different grid points with  $N_x = N_y$ 

Temperature	Mode	14 nodes /Hz	21 nodes /Hz	27 nodes /Hz	30 nodes /Hz	35 nodes /Hz
Uniform	1st	27.97	27.79	27.74	27.73	27.70
	2nd	30.51	30.56	30.32	30.17	30.13
	3rd	67.80	67.92	67.62	67.50	67.35
	4th	76.55	76.42	76.40	76.38	76.38
Non-uniform	1st	24.61	21.96	21.70	21.62	21.60
	2nd	26.17	26.40	26.27	26.21	26.07
	3rd	60.30	57.92	57.60	57.38	57.22
	4th	67.86	62.76	63.08	63.13	63.11

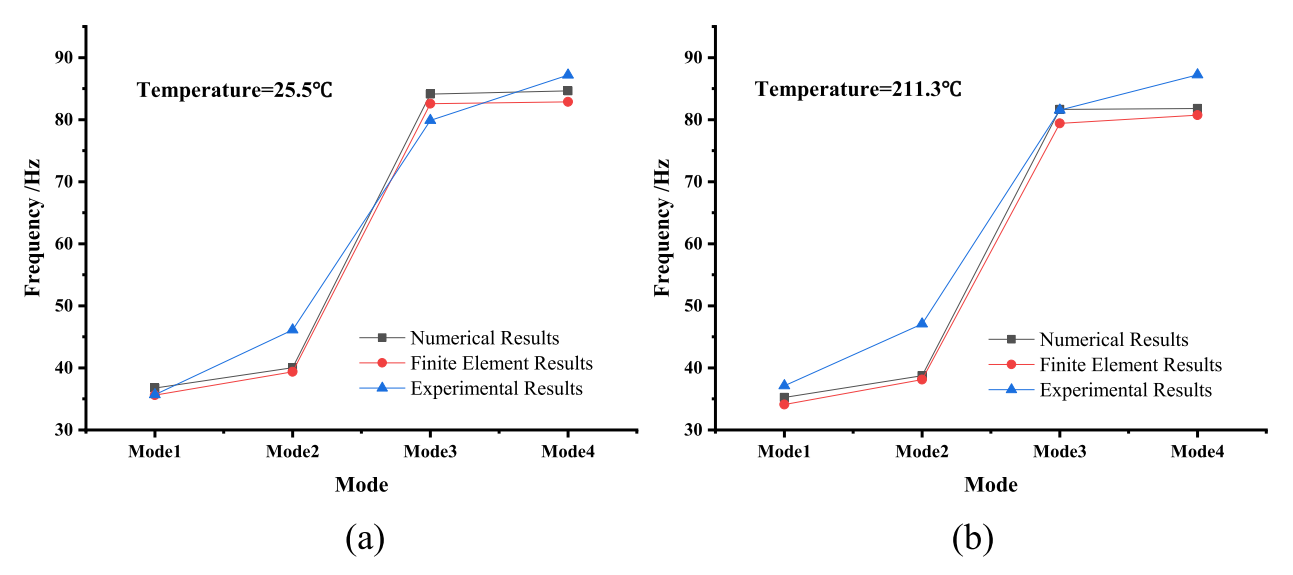


Fig. 5. First four natural frequencies of the titanium plate obtained by the present analysis, the FEM and experiments in Ref. [12], where (a) and (b) correspond to uniform temperatures of 25.5 °C and 211.3 °C, respectively

$$D\left[P_{1}\left(\sum_{k=1}^{N_{x}}A_{ik}^{(4)}\bar{w}_{kj}+2\sum_{k=1}^{N_{x}}A_{ik}^{(2)}\sum_{l=1}^{N_{y}}B_{jl}^{(2)}\bar{w}_{kl}+\sum_{l=1}^{N_{y}}B_{jl}^{(4)}\bar{w}_{il}\right)+P_{2}\sum_{k=1}^{N_{x}}A_{ik}^{(2)}\bar{w}_{kj}$$

$$+P_{3}\sum_{l=1}^{N_{y}}B_{jl}^{(2)}\bar{w}_{il}+P_{4}\sum_{k=1}^{N_{x}}A_{ik}^{(1)}\sum_{l=1}^{N_{y}}B_{jl}^{(1)}\bar{w}_{kl}+P_{5}\sum_{k=1}^{N_{x}}A_{ik}^{(3)}\bar{w}_{kj}+P_{6}\sum_{l=1}^{N_{y}}B_{jl}^{(3)}\bar{w}_{il}$$

$$+P_{7}\sum_{k=1}^{N_{x}}A_{ik}^{(1)}\sum_{l=1}^{N_{y}}B_{jl}^{(2)}\bar{w}_{kl}+P_{8}\sum_{k=1}^{N_{x}}A_{ik}^{(2)}\sum_{l=1}^{N_{y}}B_{jl}^{(1)}\bar{w}_{kl}\right]-\rho\hbar\omega^{2}\bar{w}_{ij}=0$$

$$(15)$$

where  $i = 3, 4, \dots, N_x - 3$  and  $j = 3, 4, \dots, N_y - 3$ , and

$$P_{1} = \psi(T^{*}(x, y)), P_{2} = \frac{\partial^{2} \psi(T^{*}(x, y))}{\partial x^{2}} + \frac{\partial^{2} (\psi(T^{*}(x, y) + \xi(T^{*}(x, y)))}{\partial y^{2}},$$

$$P_{3} = \frac{\partial^{2} \psi(T^{*}(x, y))}{\partial y^{2}} + \frac{\partial^{2} (\psi(T^{*}(x, y) + \xi(T^{*}(x, y)))}{\partial x^{2}}, P_{4} = -2\frac{\partial^{2} \xi(T^{*}(x, y))}{\partial x \partial y},$$

$$P_{5} = P_{7} = 2\frac{\partial \psi(T^{*}(x, y))}{\partial x}, P_{6} = P_{8} = 2\frac{\partial \psi(T^{*}(x, y))}{\partial y},$$
(16)

By rearranging Eq. (15) and considering the effect of free boundary conditions studied in this work, an assembled form is given by

$$D\mathbf{K}\mathbf{W} - ph\omega^2\mathbf{W} = \mathbf{0} \tag{17}$$

where  $\mathbf{W} = [\bar{w}_{11}, \bar{w}_{12}, \cdots, \bar{w}_{1N_x}, \cdots, \bar{w}_{i1}, \bar{w}_{i2}, \cdots, \bar{w}_{iN_x}, \cdots, \bar{w}_{N_v1}, \bar{w}_{N_v2}, \cdots, \bar{w}_{N_vN_x}]$ , and  $\mathbf{K}$  is the stiffness matrix.

The calculation process in this work is to first obtain temperature fields of the plate at different heating times as shown in Sec. 2, and then use the thermally coupled governing equation and the DQM to study thermal modal characteristics of the plate. It should be

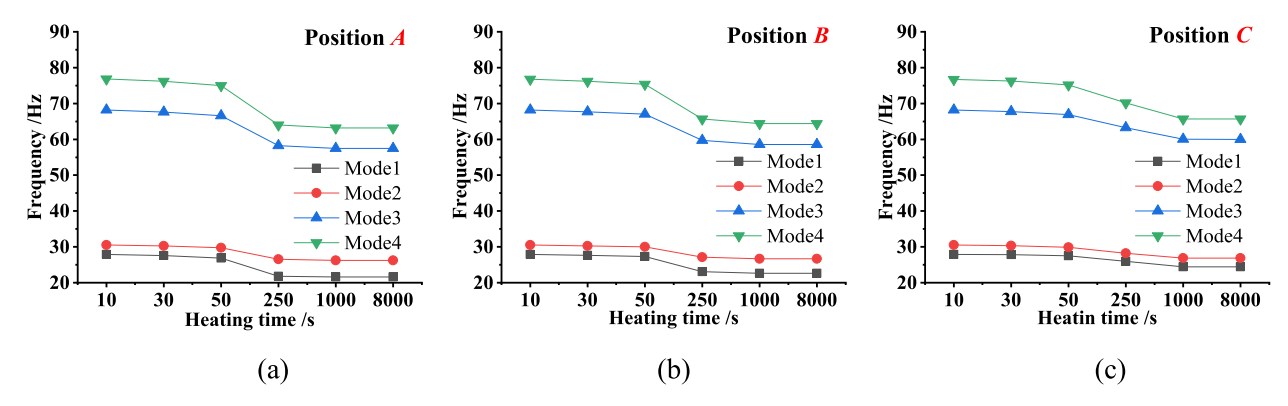


**Fig. 6.** Natural frequencies of the titanium plate under the three Gaussian heated spots *A*, *B* and *C* vs. the heating time, where (a)-(c) correspond to heated spots *A*, *B* and *C*, respectively

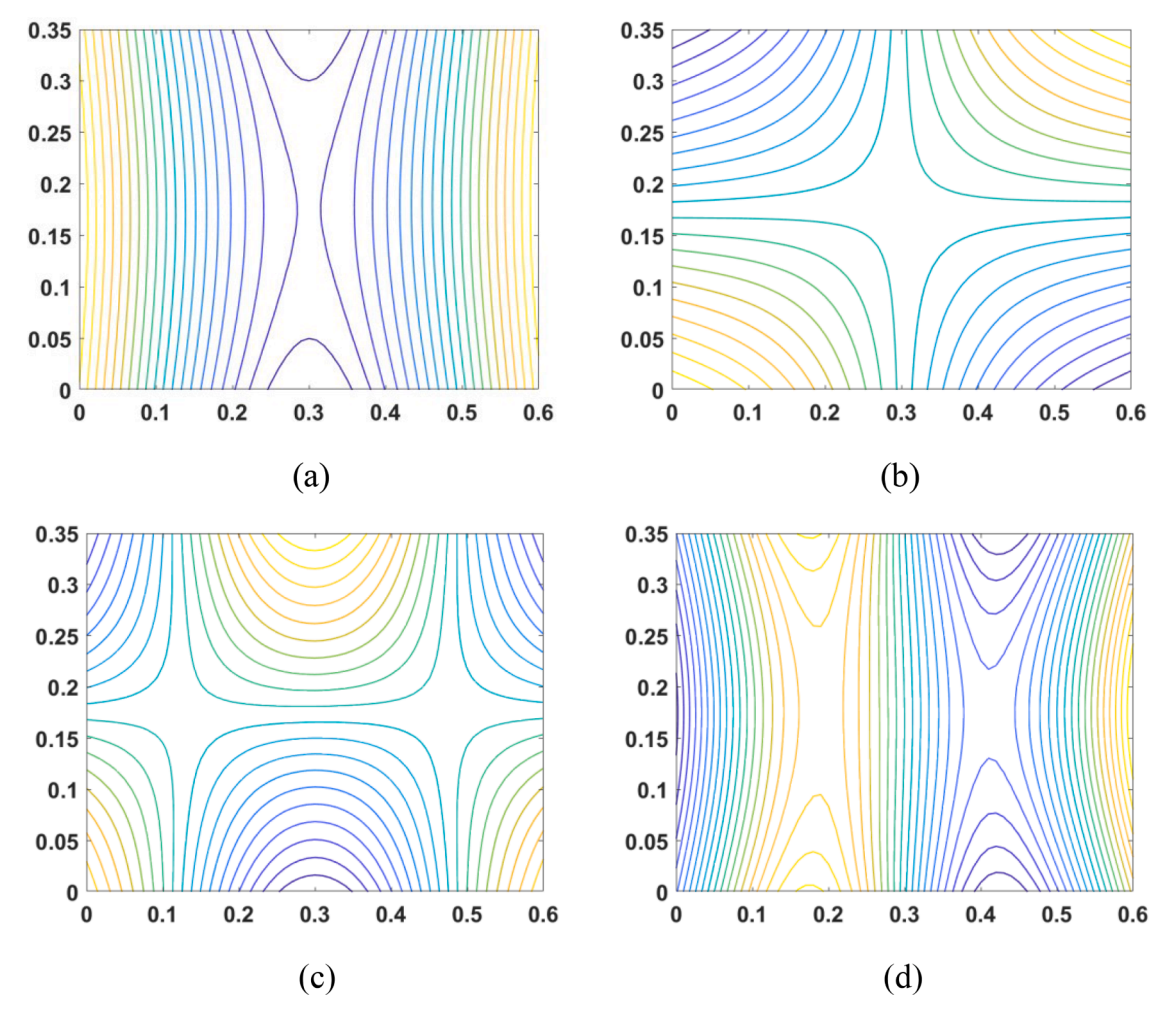


Fig. 7. Mode shapes of the titanium plate at room temperature, where (a)-(d) correspond to the first four natural frequencies, respectively

pointed out before calculating Eq. (17) by the inverse iterative method that  $\psi(T^*(x,y))$  and  $\xi(T^*(x,y))$  in Eq. (17) can be expressed by the dimensionless temperature field in Eq. (7), dimensionless temperature fields of the plate under Gaussian heat sources at different heating times can be described by Eq. (2), and their derivatives in Eq. (17) with respect to x and y can be obtained by analytical expressions. As indicated earlier, this approach can reduce violent oscillations of numerical results caused by direct use of discrete temperatures for their derivative calculations and to improve the calculation accuracy.

**Table 7**MAC values of the first four mode shapes of the titanium plate with different heating positions and times

	-	-			
Heated position	Heating time /s	1st	2nd	3rd	4th
Α	10	0.9958	0.9966	0.9996	0.9998
	30	0.9980	0.9984	0.9995	0.9947
	50	0.9966	0.9972	0.9999	0.9998
	250	0.9995	0.9995	0.9992	0.9986
	1000	0.9985	0.9987	0.9987	0.9933
	8000	0.9994	0.9995	0.9988	0.9922
В	10	0.9996	0.9997	0.9989	0.9995
	30	0.9938	0.9950	0.9989	0.9975
	50	0.9937	0.9949	0.9992	0.9968
	250	0.9944	0.9971	0.9791	0.9634
	1000	0.9959	0.9981	0.9927	0.9370
	8000	0.9930	0.9955	0.9926	0.9379
C	10	0.9958	0.9966	0.9997	0.9970
	30	0.9949	0.9956	0.9982	0.9967
	50	0.9998	0.9997	0.9991	0.9894
	250	0.9979	0.9986	0.9888	0.8960
	1000	0.9955	0.9973	0.9733	0.7308
	8000	0.9914	0.9937	0.9750	0.7362

**Table 8**Probabilities of evaluating heating positions through natural frequencies

Frequency interval /Hz	Radius interval /m	$N_{ m In}$	$N_{ m Tol}$	Probability
<21.89	< 0.058	90	99	91.0%
21.89~22.15	0.058~0.085	46	52	88.5%
22.15~22.41	0.085~0.104	25	26	96.2%
22.41~22.70	0.104~0.125	14	14	100.0%

### 4. Numerical Results of Thermal Modal Characteristics of the Titanium Plate

Before proceeding to stochastic thermal modal properties of the titanium plate, the present analyses are validated in Table 6 and Fig. 5 for the titanium plate under uniform and un-uniform temperature fields by directly comparing the present results with existing experimental ones reported in previous studies, and results from the FEM. The convergence of the proposed solution method is evaluated by varying total numbers of grid points  $N_x$  and  $N_y$  when uniform and non-uniform dimensionless temperature fields are  $T^*(x,y) = 4$  and  $T^*(x,y) = 24.64 \exp(-((x-0.2)^2 + (y-0.1)^2)/(0.338/\sqrt{3})^2) + 0.01$ , respectively. Excellent convergence can be observed from Table 6. In what follows,  $N_x = N_y = 27$  is used unless otherwise stated. Figure 5 shows the first four natural frequencies of the titanium plate with its size being 0.35 m × 0.5 m × 0.002 m, obtained by the present analysis, the FEM, and experiments shown in Ref. [12] when uniform temperatures are 25.5 °C and 211.3 °C, respectively. It can be found that the numerical method used in this work is correct. It is noted that equivalent Young's moduli  $E(T^*)$ , Poisson's ratios  $v(T^*)$ , and coefficients of thermal expansion  $\alpha(T^*)$  at different dimensionless temperatures, as shown in Table 4, are used in the following numerical simulations by use of the commercial software ANSYS, and the corresponding analysis process of ANSYS is shown in Ref. [24].

Natural frequencies of the titanium plate under three Gaussian heated spots *A*, *B* and *C*, as shown in Fig. 1, with respect to the heating time are shown in Fig. 6, where distributions of temperature fields at different heating times are given by Eq. (2) and parameters in Eq. (2) are listed in Table 3. It can be found that the first four natural frequencies have a sudden decrease phenomenon within the heating time period from 50 s to 250 s. However, in other heating time periods, the first four natural frequencies slowly decrease. The sudden decrease phenomenon is independent of the Gaussian heated spot, which is caused by thermally coupled material properties and drastic temperature field changes in the heating time period from 50 s to 250 s under the Gaussian heating source, as shown in Fig. 3. Thus, the effect of the phenomenon should be fully considered in the study of the thermodynamics of a plate.

The effect of temperature fields on modal shapes of the titanium plate is described by the modal assurance criterion (MAC), which is defined as MAC =  $\frac{(\phi_i^T\phi_a)^2}{(\phi_i^T\phi_a)(\phi_a^T\phi_a)}$ , where  $\phi_a$  and  $\phi_i$  are a modal shape at room temperature and the corresponding modal shape at a heating time, respectively. It is noted that temperature has no effect on a mode shape when the associated MAC value is equal to 1, and the smaller the value, the greater the effect of temperature on the mode shape. The first four mode shapes at room temperature of the plate are shown in Fig. 7. MAC values of the first four mode shapes of the plate at different heating positions and times are listed in Table 7. It can be found that the effect of the heating time on mode shapes of the plate is small when the heating position is relatively close to the center of the plate. Otherwise, the effect of the heating time on mode shapes of the plate is large.

Distributions of the first four natural frequencies with the Gaussian heating source and 200 random Gaussian heated spots, as listed in Table A1 in Appendix A, are shown in Figs. 8(a) and (b) when heating times are t=100 s and t=1000 s, respectively, where equipotential curves of natural frequencies and corresponding heating positions in a range of frequencies are also shown. It is noted

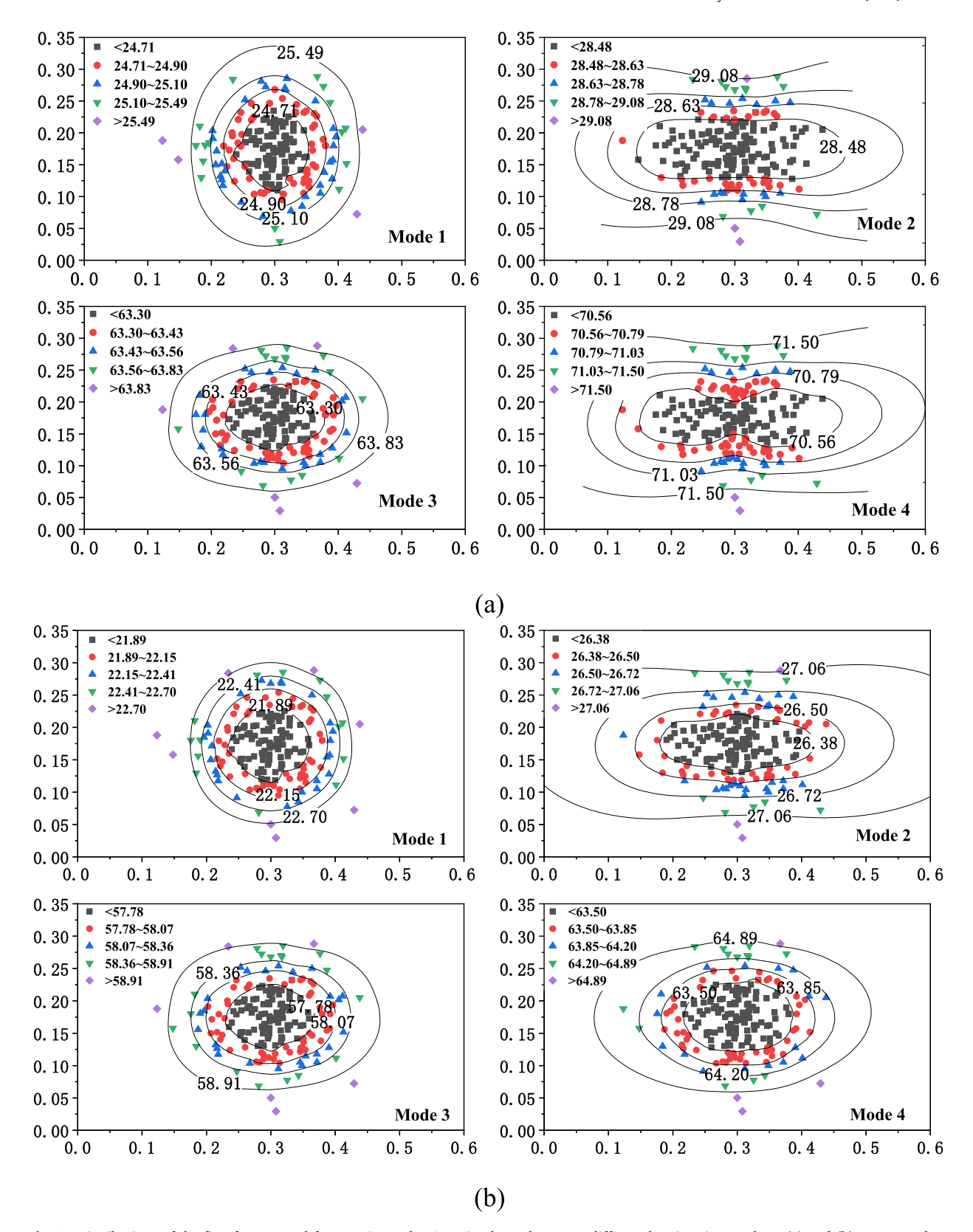


**Fig. 8.** Distributions of the first four natural frequencies under Gaussian heated spots at different heating times, where (a) and (b) correspond to heating times t=100 s and t=1000 s, respectively

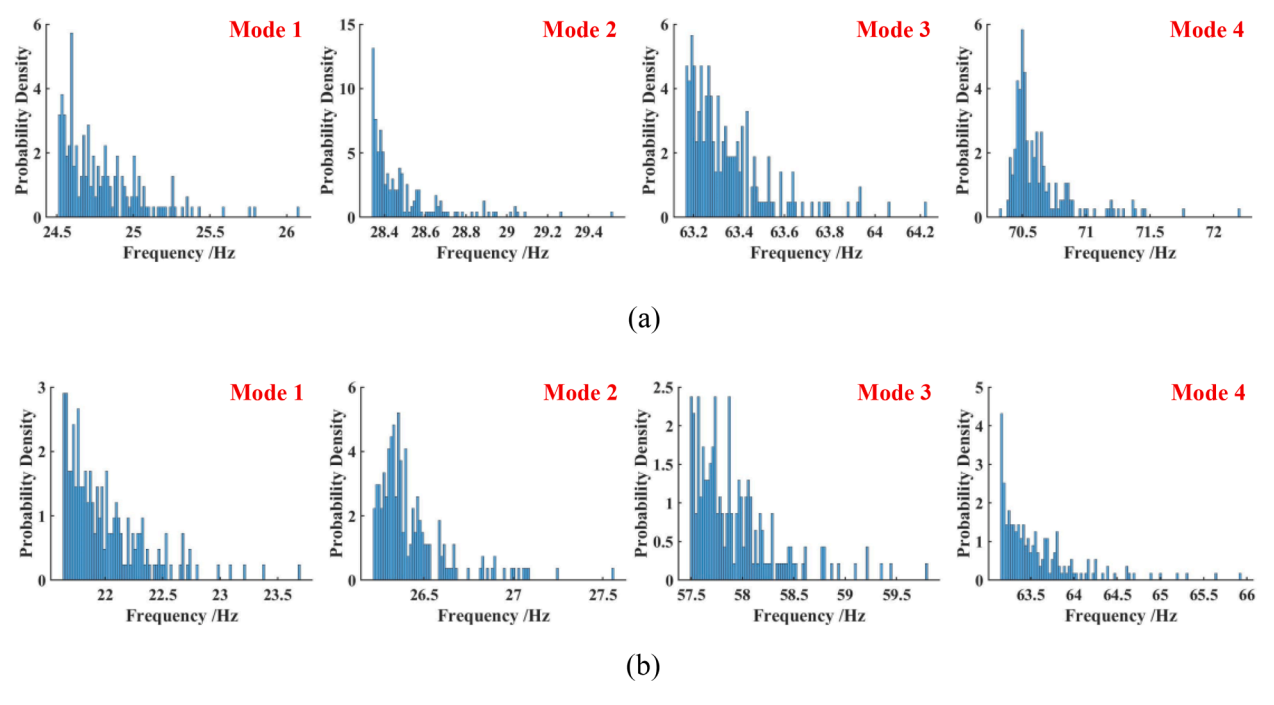


Fig. 9. Histograms of the first four natural frequencies of the titanium plate, where (a) and (b) are heating times of 100 s and 1000 s, respectively

that distributions of temperature fields of 200 random Gaussian heated spots when heating times are t=100 s and t=1000 s are given by Eq. (2), and parameters in Eq. (2) are listed Table A1 in Appendix A. It can be found that: (1) there is a strong correlation between the value of a natural frequency and the Gaussian heated spot; (2) the natural frequency is small when a Gaussian heated spot is close to the center of the titanium plate; and (3) equipotential curves of the first and third natural frequencies are approximately circles, while equipotential curves of the second and fourth natural frequencies show elliptical trends. Due to that fact, one can use the value of a natural frequency to estimate the probability of the heating position. By taking the first natural frequencies with the heating time being 1000 s into account, equipotential curves of natural frequencies, corresponding heating positions in a range of frequencies, and radii of equipotential curves are shown for mode 1 in Fig. 8(b). Probabilities of evaluating heating positions through natural frequencies are shown in Table 8, where  $[\alpha_1, \alpha_2]$  is a radius interval of equipotential curves, and  $\alpha_1$  and  $\alpha_2$  are lower and upper bounds of the interval;  $N_{\rm In}$  is the number of points with predicted values within the radius interval and frequency interval, as shown for mode 1 in Fig. 8(b); and  $N_{\rm Tol}$  is the number of points with predicted values within the frequency interval. The probability can be obtained by  $N_{\rm In}/N_{\rm Tol} \times 100\%$ . For example, in the first natural frequency of the plate with the heating time being 1000 s, when the natural frequency interval is less than 21.89 Hz, the heating source position has a 91.0% probability of being in the center circle with a radius of less than 0.058 m. It can be found that the probability of evaluating the heating position through a natural frequency can be used to estimate the uncertainty of the offset of the heating position during a dynamic experiment by a measured natural freque

By setting  $\mathbf{q} = \{q_1, q_2, \cdots, q_{200}\}$  as a certain natural frequency with 200 sample data at a certain time, as shown in Figs. 8(a) and (b), letting  $q_{\min}$  and  $q_{\max}$  be the minimum and maximum values in  $\mathbf{q}$ , and evenly dividing the interval  $[q_{\min}, q_{\max}]$  into  $\bar{n}$  subintervals, the ith subinterval can be expressed as

$$L_{i} = \left[\frac{i-1}{\bar{n}}(q_{\max} - q_{\min}) + q_{\min}, \frac{i}{\bar{n}}(q_{\max} - q_{\min}) + q_{\min}\right), i = 1, 2, \dots, \bar{n} - 1$$
(18a)

and

$$L_n = \left[\frac{\bar{n} - 1}{\bar{n}}(q_{\text{max}} - q_{\text{min}}) + q_{\text{min}}, q_{\text{max}}\right]$$

$$\tag{18b}$$

The probability density  $PD_i$  of each subinterval  $L_i$ , where  $i = 1, 2, \dots, \bar{n}$ , can be calculated by

$$PD_i = \frac{N_{\text{num}}}{200} \frac{\bar{n}}{q_{\text{max}} - q_{\text{min}}} \tag{19}$$

where  $N_{\text{num}}$  is the number of the value of a natural frequency in the ith subinterval, and  $\bar{n}$ =100 is used in this work. Histograms of the first four natural frequencies of the titanium plate with 200 random Gaussian heated spots at different times, as shown in Table A1 in Appendix A, are shown in Fig. 9.

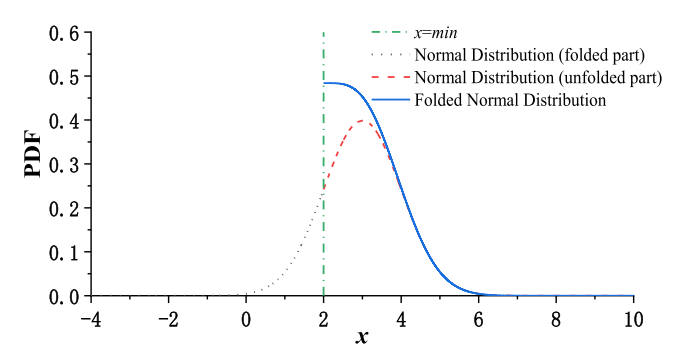


Fig. 10. Folded normal distribution

# 5. Random Small Sample Estimation of Thermal Modal Properties of the Titanium Plate Induced by a Random Heating Position

A random small sample estimation method is used in this section to study distributions of the first four natural frequencies of the titanium plate induced by a random heating position. First, by considering that sample data of the first four natural frequencies with 200 random Gaussian heated spots at heating times of 100 s and 1000 s, as shown in Fig. 8, are small, an improved Bootstrap method is used to expand sample data. Second, folded normal distribution is used to describe distributions of the first four natural frequencies of the titanium plate at heating times of 100 s and 1000 s according to histograms in Fig. 9. Finally, PDFs of natural frequencies and their confidence intervals are obtained.

### 5.1. Folded Normal Distribution and Improved Bootstrap Method

Let  $Y \sim N(\mu, \sigma^2)$  and X = |Y - min| + min, where min is the minimum value in sample data; the PDF of  $Y \sim FN(\mu, \sigma^2)$  can be expressed as [25]

$$f(x) = \frac{1}{\sqrt{2\pi\sigma^2}} \left( \exp\left(-\frac{1}{2\sigma^2}(x-\mu)^2\right) + \exp\left(-\frac{1}{2\sigma^2}(2min - x - \mu)^2\right) \right)$$
 (20)

where  $N(\mu, \sigma^2)$  and  $FN(\mu, \sigma^2)$  are the normal distribution and folded normal distribution, respectively;  $\mu$  and  $\sigma^2$  are the mathematical expectation and variance, respectively; and x = min is a folded axis of the PDF that can be described by Fig. 10.

It is difficult to directly use the Monte Carlo method to analyze thermal modal characteristics of the titanium plate induced by a random heating position due to a large amount of calculation in thermal field analyses. Therefore, with existing random small sample data, an improved Bootstrap method is used to expand sample data [26], which overcomes the limitation of the previous Bootstrap method that only relies on existing observation information, and resampled sample data can only be generated by original samples [26]. The Bootstrap method is only dependent on existing observation information and has no prior property in calculation, which can be conveniently applied to data processing. However, calculation in the Bootstrap method limits the range of the self-help sample that is only from the original sample data, which makes it impossible to obtain distribution characteristics outside non-observed sample data. Although the Bootstrap method can increase observation data through the self-help sample, no new observation information is actually added. In this case, the self-help sample may lose its proper significance and characteristics. However, the improved Bootstrap method can obtain the self-help sample that is completely different from the original sample based on minimizing the deviation from the real distribution. Such a method can obtain information outside observation data. It should be noted that the method cannot obtain accurate information beyond observation data, but only approximate information [26]. The specific implementation process of the improved Bootstrap method is shown below.

Arranging 200 sample data of a certain natural frequency at a certain time  $\mathbf{q} = \{q_1, q_2, \cdots, q_{200}\}$  in the ascending order, one can record them as  $\mathbf{P} = \{p_1, p_2, \cdots, p_{200}\}$ . A neighborhood  $U_i = [a_i, b_i]$  for each  $p_i$  can be expressed as

$$\begin{cases}
U_{1} = [p_{1} - (p_{2} - p_{1})/m, p_{1} + (p_{2} - p_{1})/m] \\
\vdots \\
U_{i} = [p_{i} - (p_{i} - p_{i-1})/m, p_{i} + (p_{i+1} - p_{i})/m] \\
\vdots \\
U_{n} = [p_{n} - (p_{n} - p_{n-1})/m, p_{n} + (p_{n} - p_{n-1})/m]
\end{cases} (21)$$

where  $m \ge 2$  and  $i = 2, 3, \dots n - 1$  with n = 200; m = 2 is used in this work.

By assuming that N is the number of resampling times, the following rules are used to expand sample data:

(1) Determine a subscript sample I of an expanded neighborhood, which satisfies uniform distribution in the interval [1, 200]. The probability of l = i is

**Table 9**Original parameters and fitted parameters of folded normal distribution obtained by the improved Bootstrap method

$\mu_o$	$\sigma_o^2$	min	$\mu_{\alpha}$	$\sigma_{\alpha}^2$	$arepsilon_{\mu}$ /%	$\varepsilon_{\sigma^2}$ /%
35	0.09	34.9	34.90	0.0897	0.286	0.333
45	0.25	40.0	45.05	0.2540	0.111	1.600
55	0.04	54.8	55.00	0.0378	0.000	5.500
65	0.25	66.0	65.03	0.2578	0.046	3.120

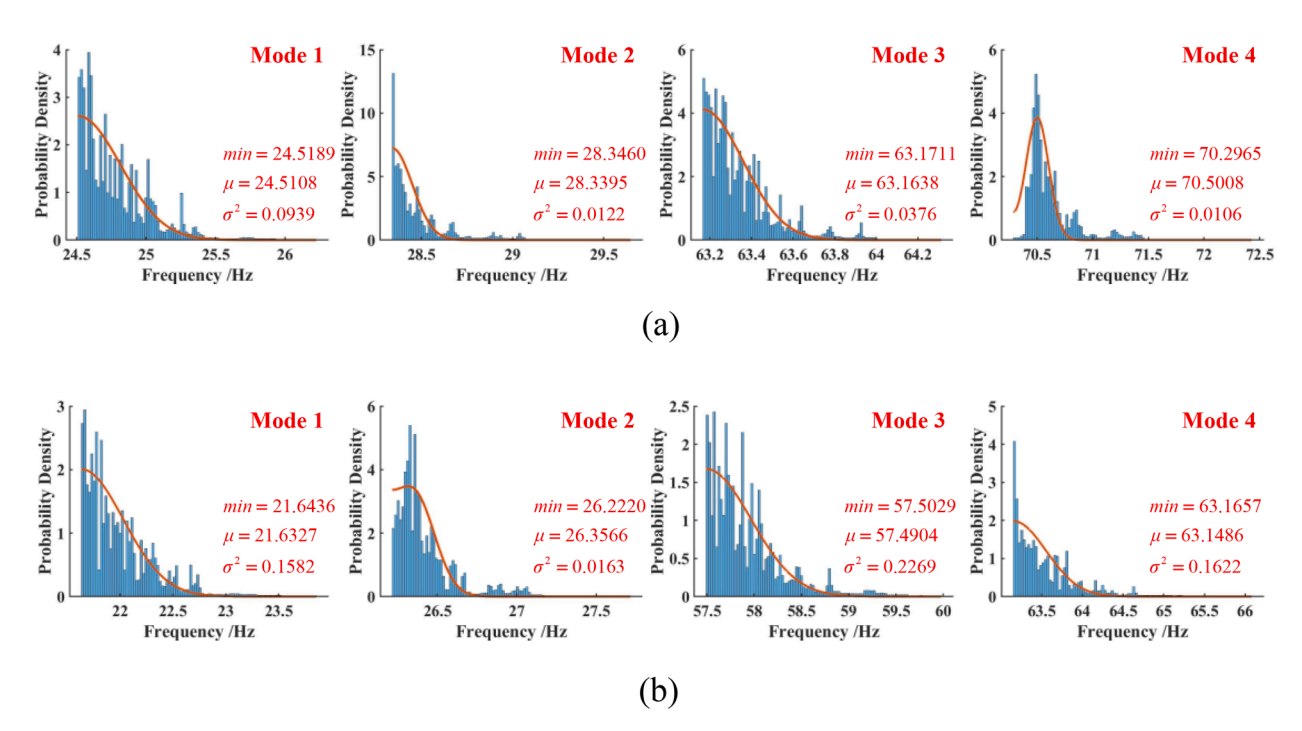


Fig. 11. Histograms and their PDFs of the re-sampled first four natural frequencies of the titanium plate, where (a) and (b) correspond to heating times of 100 s and 1000 s, respectively

$$P(l=i) = \frac{1}{n} \tag{22}$$

By resampling the subscript in  $U_i N$  times according to the above distribution, a sample  $\mathbf{l} = \{l_1, l_2, \dots, l_N\}$  can be obtained, where  $l_i$  is an integer in the interval [1, 200].

(2) Self-help sample  $\mathbf{Q}_{i}^{*}$ :

$$\mathbf{Q}_{i}^{*} \sim U\left(U_{l_{i}}\right), i=1, 2\cdots N \tag{23}$$

where  $U(U_{l_i}) = U([a_i,b_i])$  is uniform distribution in the interval  $[a_i,b_i]$ . By use of such a method, the expanded observation sample  $\mathbf{q}^* = \{q_1^*,q_2^*,\cdots,q_N^*\}$  can be obtained by the self-help sample  $\mathbf{Q}^* = \{Q_1^*,Q_2^*,\cdots,Q_N^*\}$ . Such a method extends distribution characteristics of data to its non-observed samples while keeping original distribution characteristics as consistent as possible.

In order to verify the feasibility of the above sampling method, folded normal distribution with different parameters is verified:

- (1) Generate a sample  $\mathbf{q}_o$  with a sample size of 200, which obeys folded distribution with the mean  $\mu_o$ , variance  $\sigma_o^2$ , and minimum value *min*.
- (2) An expanded sample  $\mathbf{q}_{\alpha}$  can be obtained by the improved Bootstrap method with 4000 times of sampling of the sample  $\mathbf{q}_{o}$ .
- (3) Fit the PDF of  $\mathbf{q}_a$  by use of folded distribution to obtain the fitted mean  $\mu_a$  and variance  $\sigma_a^2$ .

Based on the improved Bootstrap method, verification results are shown in Table 9. It can be found that relative errors of the mean  $\varepsilon_{\mu}$  and variance  $\varepsilon_{\sigma^2}$  are small, and such a method can be used in random small sample estimation.

**Table 10**Values of the parameter *min* and fitted results in folded normal distribution

Heating time /s	Mode	min /Hz	μ/Hz	$\sigma^2$ /Hz $^2$
100	1st	24.5189	24.5108	0.0939
	2nd	28.3460	28.3395	0.0122
	3rd	63.1711	63.1638	0.0376
	4th	70.2965	70.5008	0.0106
1000	1st	21.6436	21.6327	0.1582
	2nd	26.2220	26.3566	0.0163
	3rd	57.5029	57.4904	0.2269
	4th	63.1657	63.1486	0.1622

**Table 11**Confidence intervals of the first four natural frequencies of the titanium plate when heating times are 100 s and 1000 s

Heating time /s	Mode	Confidence interval for $\eta{=}3$ /Hz	confidence interval for $\eta{=}2$ /Hz	confidence interval for $\eta = 1$ /Hz
100	1	[24.5189, 25.4286]	[24.5189, 25.1336]	[24.5189, 24.8254]
	2	[28.3460, 28.6745]	[28.3460, 28.5679]	[28.3460, 28.4567]
	3	[63.1711, 63.7471]	[63.1711, 63.5601]	[63.1711, 63.3652]
	4	[70.2965, 70.7836]	[70.2965, 70.6754]	[70.3978, 70.6032]
1000	1	[21.6436, 22.8245]	[21.6436, 22.4412]	[21.6436, 22.0415]
	2	[26.2220, 26.7074]	[26.2220, 26.5732]	[26.2289, 26.4278]
	3	[57.5029, 58.9175]	[57.5029, 58.4581]	[57.5029, 57.9794]
	4	[63.1657, 64.3620]	[63.1657, 63.9738]	[63.1657, 63.5688]

### 5.2. Numerical results

According to the above improved Bootstrap method, the first four natural frequencies of the titanium plate with 200 random Gaussian heated spots at heating times of 100 s and 1000 s, as shown in Fig. 8, are resampled 4000 times, and their histograms are shown in Fig. 10. Folded normal distribution given by Eq. (20) is used to describe their PDFs, as shown in Fig. 11, where the parameter *min* in Eq. (20) takes the minimum value in sample data. Values of the parameter *min* and fitted results in folded normal distribution are shown in Table 10. It can be found from Table 10 that: (1) the variance corresponding to each natural frequencies increases with the heating time, which shows that the random heating position has a great effect on natural frequencies of the plate when the heating time increases. (2) Variances corresponding to the first and second natural frequencies of the plate are the largest when heating times are 100 s and 1000 s, respectively. This also shows that the effect of the random heating position on the first and second natural frequencies is larger than that on the other natural frequencies when heating times are 100 s and 1000 s, respectively.

Considering that folded distribution is a variant of normal distribution, one can study confidence intervals of natural frequencies of the titanium plate induced by the random heating position from the 3-sigma criterion with some modifications. By letting  $X \in [min, +\infty)$  when  $X \sim NF(\mu, \sigma^2)$ , lower bounds of confidence intervals  $\chi$  can be defined as

$$\chi = \begin{cases} \mu - \eta \sigma, & \min \le \mu - \eta \sigma \\ \min, & \min > \mu - \eta \sigma \end{cases}$$
 (24)

where  $\eta=1,2,3$  correspond to three conditions whose confidences are 0.683, 0.955 and 0.997, respectively. Thus, upper bounds of confidence intervals can be obtained by PDFs in Eq. (20) with parameters in Table 10. Confidence intervals for  $\eta=1,2,3$  are given in Table 11. It is noted that confidence intervals can be used to estimate reliability of thermal modal experiments when measured natural frequencies are obtained. If measured natural frequencies fall within a confidence interval, it can be believed that the random heating position affects thermal modal experiments. If they do not, it means that there are errors in thermal modal experiments or there are other important uncertainties that have not been considered in the analysis.

### 6. Conclusions

Stochastic thermal modal characteristics of a titanium plate induced by a random heating position are studied by a random small sample estimation method that combines the improved Bootstrap method and folded normal distribution. The research mainly includes the following work: (1) temperature distributions of the plate under two-parameter Gaussian heating sources with different heated spots are obtained by a simulation method, and a modified Gaussian function is used to describe temperature fields to reduce violent oscillations of numerical results caused by direct use of discrete temperatures for their derivative calculations and to improve the calculation accuracy. (2) A coupled thermal dynamic governing equation of the plate is established by a thermally coupled constitutive relation theory, and modal parameters of the plate at different high temperatures are obtained by the DQM. By comparing the present numerical results with those from the FEM and experimental results, the accuracy of the numerical results is verified. (3) The first four natural frequencies of the plate under 200 Gaussian heating sources with different heating positions and times are obtained. By use of the improved Bootstrap method to expand sample data of natural frequencies, folded normal distribution is used to

**Table 1A**Positions of heated spots and fitted parameters of temperature fields

No.	<i>x</i> /m	y/m	Heating time	Heating time=100 s			Heating time=1000 s	
			$T_Q$	$R_Q/m$	$d_Q$	$T_Q$	$R_Q/m$	$d_Q$
1	0.247	0.179	20.954	0.260	0.000	24.560	0.346	0.000
2	0.347	0.128	20.944	0.259	0.000	24.527	0.347	0.000
3	0.318	0.196	20.911	0.260	0.000	23.149	0.336	1.372
4	0.299	0.209	20.910	0.260	0.000	22.630	0.330	1.907
5	0.309	0.218	20.917	0.259	0.000	22.936	0.333	1.589
6	0.222	0.140	21.001	0.258	0.000	24.666	0.342	0.000
7	0.296	0.197	20.906	0.260	0.000	22.527	0.329	2.015
8	0.380	0.180	21.001	0.259	0.000	24.682	0.342	0.000
9	0.305	0.216	20.915	0.260	0.000	22.792	0.331	1.738
10	0.302	0.202	20.907	0.260	0.000	22.542	0.329	1.999
11	0.263	0.220	20.940	0.259	0.000	24.492	0.348	0.000
12	0.298	0.168	20.902	0.260	0.000	22.380	0.328	2.168
13	0.312	0.168	20.904	0.260	0.000	22.709	0.331	1.828
14	0.321	0.225	20.916	0.259	0.000	23.666	0.340	0.835
15	0.281	0.069	20.948	0.257	0.000	24.257	0.343	0.217
16	0.288	0.150	20.909	0.260	0.000	22.833	0.332	1.697
17	0.401	0.111	21.056	0.257	0.000	24.747	0.338	0.000
18	0.187	0.156	21.082	0.257	0.000	24.821	0.336	0.000
19	0.411	0.207	21.079	0.257	0.000	24.809	0.337	0.000
20	0.317	0.216	20.919	0.259	0.000	23.292	0.337	1.221
21	0.350	0.124	20.919	0.259	0.000	24.539	0.346	0.000
22	0.217	0.151	21.010	0.259	0.000	24.692	0.341	0.000
23	0.270	0.131	20.918	0.260	0.000	24.092	0.345	0.408
24	0.286	0.160	20.917	0.260	0.000	22.873	0.333	1.657
25	0.321	0.100	20.912	0.260	0.000	23.395	0.338	1.118
26	0.321	0.190	21.010	0.259	0.000	23.395 24.695		0.000
27	0.324	0.195	20.927		0.000	23.778	0.341 0.341	0.720
				0.259				
28	0.239	0.166	20.968	0.259	0.000	24.592	0.345	0.000
29	0.303	0.068	20.943	0.257	0.000	24.006	0.341	0.474
30	0.333	0.232	20.930	0.259	0.000	24.453	0.348	0.028
31	0.316	0.144	20.914	0.260	0.000	23.156	0.335	1.363
32	0.354	0.115	20.962	0.258	0.000	24.553	0.345	0.000
33	0.350	0.162	20.949	0.260	0.000	24.547	0.347	0.000
34	0.267	0.104	20.938	0.258	0.000	24.479	0.347	0.000
35	0.313	0.174	20.904	0.260	0.000	22.769	0.332	1.765
36	0.253	0.147	20.948	0.259	0.000	24.533	0.347	0.000
37	0.234	0.284	21.000	0.256	0.000	24.589	0.342	0.000
38	0.346	0.232	20.948	0.259	0.000	24.524	0.346	0.000
39	0.300	0.050	20.955	0.256	0.000	24.309	0.343	0.162
40	0.297	0.197	20.905	0.260	0.000	22.498	0.329	2.045
41	0.346	0.105	20.953	0.258	0.000	24.519	0.346	0.000
42	0.330	0.162	20.919	0.260	0.000	24.113	0.345	0.382
43	0.318	0.183	20.908	0.260	0.000	23.093	0.335	1.430
44	0.363	0.212	20.968	0.259	0.000	24.595	0.345	0.000
45	0.346	0.161	20.943	0.260	0.000	24.531	0.347	0.000
46	0.312	0.254	20.928	0.258	0.000	23.641	0.339	0.854
47	0.265	0.151	20.928	0.260	0.000	24.487	0.349	0.000
48	0.267	0.191	20.907	0.260	0.000	23.925	0.344	0.570
49	0.360	0.208	20.961	0.259	0.000	24.583	0.345	0.000
50	0.219	0.179	21.002	0.259	0.000	24.684	0.342	0.000
51	0.299	0.219	20.916	0.259	0.000	22.790	0.331	1.739
52	0.203	0.191	21.044	0.258	0.000	24.758	0.339	0.000
53	0.351	0.136	20.947	0.259	0.000	24.546	0.346	0.000
54	0.343	0.085	20.960	0.257	0.000	24.510	0.345	0.000
55	0.300	0.268	20.935	0.257	0.000	23.740	0.339	0.750
56	0.296	0.145	20.909	0.260	0.000	22.604	0.330	1.934
57	0.176	0.180	21.109	0.257	0.000	24.866	0.335	0.000
58	0.329	0.203	20.923	0.260	0.000	24.090	0.345	0.404
59	0.190	0.181	21.074	0.258	0.000	24.811	0.337	0.000
60	0.184	0.130	21.088	0.257	0.000	24.818	0.336	0.000
61	0.258	0.199	20.938	0.260	0.000	24.512	0.348	0.000
62	0.235	0.160	20.978	0.259	0.000	24.611	0.344	0.000
63	0.330	0.213	20.928	0.259	0.000	24.160	0.345	0.330
64	0.182	0.210	21.094	0.257	0.000	24.832	0.336	0.000
65	0.298	0.195	20.905	0.260	0.000	22.469	0.328	2.075
66	0.304	0.170	20.902	0.260	0.000	22.409	0.328	2.138
		0.142	20.940	0.259			0.348	0.000

(continued on next page)

Table 1A (continued)

No.	x /m	y/m	Heating time	=100 s		Heating time		
	•	• /			$d_Q$	$T_Q$ $R_Q$ /m		$d_Q$
68	0.318	0.142	20.916	0.260	0.000	23.268	0.337	1.248
69	0.316	0.270	20.940	0.257	0.000	24.025	0.342	0.457
70	0.372	0.105	20.997	0.258	0.000	24.620	0.342	0.000
71	0.216	0.126	21.016	0.258	0.000	24.683	0.341	0.000
72	0.253	0.151	20.946	0.260	0.000	24.533	0.347	0.000
73	0.247	0.232	20.959	0.258	0.000	24.551	0.345	0.000
74	0.273	0.148	20.920	0.260	0.000	23.901	0.343	0.597
75	0.236	0.124	20.975	0.258	0.000	24.594	0.344	0.000
76	0.354	0.124	20.957	0.259	0.000	24.553	0.346	0.000
77	0.302	0.212	20.912	0.260	0.000	22.681	0.330	1.853
78	0.300	0.221	20.917	0.259	0.000	22.816	0.332	1.712
79	0.316	0.154	20.910	0.260	0.000	23.026	0.334	1.498
30	0.267	0.225	20.927	0.259	0.000	24.477	0.348	0.005
31	0.208	0.171	21.029	0.258	0.000	24.734	0.340	0.000
32	0.286	0.222	20.921	0.259	0.000	23.193	0.335	1.322
33	0.295	0.142	20.910	0.260	0.000	22.661	0.330	1.875
34	0.279	0.281	20.949	0.257	0.000	24.335	0.344	0.138
15	0.438	0.205	21.134	0.256	0.000	24.902	0.333	0.000
86	0.299	0.174	20.901	0.260	0.000	22.368	0.328	2.18
7	0.275	0.187	20.914	0.260	0.000	23.694	0.341	0.811
88	0.390	0.128	21.031	0.258	0.000	24.713	0.340	0.000
19	0.297	0.112	20.916	0.259	0.000	23.149	0.334	1.365
90	0.348	0.100	20.960	0.258	0.000	24.528	0.345	0.000
1	0.308	0.029	20.970	0.255	0.000	24.482	0.342	0.000
92	0.254	0.185	20.941	0.260	0.000	24.530	0.347	0.000
93	0.377	0.273	21.014	0.256	0.000	24.630	0.341	0.000
4	0.289	0.131	20.918	0.259	0.000	23.023	0.334	1.498
5	0.319	0.173	20.908	0.260	0.000	23.180	0.336	1.34
6	0.215	0.132	21.019	0.258	0.000	24.694	0.341	0.00
7	0.387	0.154	21.019	0.258	0.000	24.711	0.341	0.00
8	0.329	0.204	20.924	0.260	0.000	24.096	0.345	0.397
19	0.392	0.207	21.033	0.258	0.000	24.729	0.340	0.000
00	0.292	0.246	20.922	0.258	0.000	23.402	0.337	1.102
.01	0.312	0.095	20.929	0.258	0.000	23.655	0.339	0.839
.02	0.233	0.200	20.974	0.259	0.000	24.620	0.344	0.000
03	0.298	0.235	20.914	0.259	0.000	23.082	0.334	1.43
.04	0.256	0.151	20.942	0.260	0.000	24.521	0.347	0.00
105	0.287	0.223	20.921	0.259	0.000	23.172	0.335	1.34
106	0.260	0.139	20.941	0.259	0.000	24.506	0.348	0.00
.07	0.302	0.218	20.915	0.259	0.000	22.780	0.331	1.749
.08	0.351	0.142	20.955	0.259	0.000	24.545	0.346	0.000
109	0.346	0.122	20.945	0.259	0.000	24.523	0.347	0.000
110	0.248	0.122	20.954	0.259	0.000	24.552	0.346	0.000
111	0.317	0.268	20.939	0.257	0.000	24.032	0.342	0.450
12	0.123	0.188	21.186	0.255	0.000	25.002	0.328	0.000
13	0.123	0.188	20.941	0.257	0.000	24.017	0.342	0.464
.14	0.319	0.275	20.950	0.256	0.000	24.320	0.344	0.46
115	0.304	0.283	20.902	0.260	0.000	22.408	0.328	2.140
16	0.397	0.172	21.042	0.258	0.000	24.753	0.339	0.00
17	0.367	0.194	21.042	0.256	0.000	24.593	0.341	0.00
			20.971	0.259		24.588	0.345	0.00
18	0.360	0.150			0.000	23.560		
19	0.278	0.203	20.917	0.260	0.000		0.340	0.94
20	0.242	0.184	20.963	0.259	0.000	24.581	0.346	0.00
21	0.309	0.182	20.903	0.260	0.000	22.596	0.330	1.94
22	0.314	0.104	20.924	0.258	0.000	23.565	0.338	0.93
23	0.285	0.179	20.906	0.260	0.000	22.886	0.333	1.64
.24	0.358	0.182	20.963	0.259	0.000	24.581	0.346	0.00
.25	0.293	0.158	20.905	0.260	0.000	22.551	0.329	1.99
126	0.333	0.232	20.931	0.259	0.000	24.474	0.348	0.00
127	0.429	0.072	21.102	0.255	0.000	24.820	0.334	0.00
128	0.298	0.150	20.907	0.260	0.000	22.527	0.329	2.01
29	0.313	0.210	20.914	0.260	0.000	22.981	0.334	1.54
30	0.253	0.252	20.959	0.258	0.000	24.523	0.345	0.00
131	0.319	0.185	20.909	0.260	0.000	23.179	0.336	1.34
132	0.299	0.211	20.912	0.260	0.000	22.666	0.330	1.869
133	0.330	0.186	20.919	0.260	0.000	24.128	0.345	0.365
134	0.329	0.185	20.918	0.260	0.000	24.048	0.345	0.448
135	0.260	0.202	20.937	0.260	0.000	24.507	0.348	0.000

(continued on next page)

Table 1A (continued)

No.	<i>x</i> /m	y/m	Heating time=100 s			Heating time=1000 s		
			$T_Q$	$R_Q$ /m	$d_Q$	$T_Q$	$R_Q$ /m	$d_Q$
136	0.289	0.110	20.919	0.259	0.000	23.369	0.337	1.13
137	0.327	0.155	20.918	0.260	0.000	23.854	0.343	0.64
138	0.228	0.173	20.992	0.259	0.000	24.643	0.343	0.00
139	0.307	0.131	20.917	0.259	0.000	22.889	0.332	1.63
140	0.283	0.220	20.922	0.259	0.000	23.372	0.337	1.13
141	0.291	0.180	20.903	0.260	0.000	22.565	0.330	1.97
142	0.294	0.119	20.912	0.259	0.000	23.063	0.334	1.45
143	0.218	0.117	21.014	0.258	0.000	24.669	0.341	0.00
144	0.278	0.106	20.928	0.258	0.000	23.921	0.342	0.56
145	0.349	0.128	20.947	0.259	0.000	24.536	0.346	0.00
	0.207	0.128		0.258	0.000	24.736	0.340	0.00
146			21.034					
147	0.338	0.167	20.928	0.260	0.000	24.498	0.348	0.00
148	0.391	0.157	21.029	0.258	0.000	24.731	0.340	0.00
149	0.280	0.130	20.923	0.259	0.000	23.524	0.339	0.98
150	0.334	0.244	20.939	0.258	0.000	24.484	0.347	0.00
151	0.196	0.185	21.059	0.258	0.000	24.786	0.338	0.00
152	0.350	0.234	20.954	0.258	0.000	24.535	0.346	0.00
153	0.225	0.147	20.992	0.259	0.000	24.655	0.343	0.00
154	0.316	0.136	20.918	0.260	0.000	23.205	0.336	1.31
155	0.282	0.175	20.908	0.260	0.000	23.155	0.336	1.36
156	0.288	0.159	20.906	0.260	0.000	22.796	0.332	1.73
157	0.376	0.190	20.992	0.259	0.000	24.663	0.342	0.00
158	0.387	0.248	21.028	0.257	0.000	24.684	0.340	0.00
159	0.326	0.162	20.916	0.260	0.000	23.805	0.342	0.69
160	0.293	0.216	20.915	0.260	0.000	22.848	0.332	1.6
161	0.286	0.135	20.917	0.260	0.000	23.133	0.335	1.3
162	0.307	0.118	20.913	0.259	0.000	23.102	0.334	1.4
163	0.202	0.203	21.047	0.258	0.000	23.695	0.340	0.8
164	0.283	0.105	20.926	0.258	0.000	23.695	0.340	0.8
165	0.406	0.202	21.065	0.258	0.000	24.789	0.338	0.0
166	0.233	0.195	20.983	0.259	0.000	24.618	0.344	0.0
167	0.372	0.118	20.993	0.258	0.000	24.626	0.343	0.0
168	0.364	0.250	20.985	0.257	0.000	24.587	0.343	0.0
169	0.315	0.194	20.909	0.260	0.000	22.992	0.334	1.5
170	0.286	0.120	20.915	0.259	0.000	23.341	0.337	1.1
171	0.326	0.077	20.947	0.257	0.000	24.379	0.345	0.0
172	0.413	0.152	21.082	0.257	0.000	20.205	0.650	0.0
173	0.291	0.164	20.904	0.260	0.000	22.616	0.330	1.9
174	0.392	0.180	21.031	0.258	0.000	24.738	0.340	0.0
175	0.324	0.191	20.914	0.260	0.000	23.640	0.341	0.8
176	0.298	0.263	20.932	0.258	0.000	23.640	0.338	0.8
177	0.378	0.138	21.000	0.258	0.000	24.663	0.342	0.0
178	0.264	0.189	20.927	0.260	0.000	24.493	0.349	0.0
179	0.298	0.176	20.901	0.260	0.000	22.375	0.328	2.1
180	0.309	0.181	20.903	0.260	0.000	22.578	0.330	1.9
181	0.304	0.110	20.918	0.259	0.000	23.220	0.335	1.2
182	0.366	0.226	20.980	0.258	0.000	24.606	0.344	0.0
183	0.330	0.121	20.926	0.259	0.000	24.235	0.346	0.2
184	0.289	0.117	20.915	0.259	0.000	23.252	0.336	1.2
185	0.247	0.091	20.970	0.257	0.000	24.542	0.344	0.0
186	0.263	0.246	20.943	0.258	0.000	24.491	0.347	0.0
	0.346	0.204	20.946	0.259	0.000	24.527	0.347	0.0
87								
188	0.359	0.173	20.965	0.259	0.000	24.587	0.345	0.0
189	0.380	0.180	20.999	0.259	0.000	24.680	0.342	0.0
190	0.273	0.202	20.921	0.260	0.000	23.906	0.343	0.5
191	0.260	0.128	20.934	0.259	0.000	24.502	0.347	0.0
192	0.364	0.146	20.969	0.259	0.000	24.605	0.344	0.0
193	0.274	0.155	20.917	0.260	0.000	23.809	0.342	0.6
194	0.362	0.230	20.974	0.258	0.000	24.587	0.344	0.0
195	0.148	0.158	21.160	0.256	0.000	24.947	0.331	0.0
196	0.311	0.166	20.904	0.260	0.000	22.705	0.331	1.8
197	0.329	0.214	20.928	0.259	0.000	24.142	0.345	0.3
198	0.298	0.158	20.904	0.260	0.000	22.445	0.328	2.1
199	0.242	0.221	20.962	0.259	0.000	24.571	0.345	0.0
4.5	0.289	0.195	20.907	0.260	0.000	22.766	0.332	1.7

obtain stochastic characteristics of natural frequencies of the plate induced by a random position based on expanded sample data. In summary, this work proposes a complete statistical analysis process for thermodynamic problems with small sample data. Relevant research will be of great significance to reliability evaluation of thermodynamic experimental results, and error analysis between experimental and theoretical results.

### CRediT authorship contribution statement

**Yu-Jia Hu:** Conceptualization, Methodology, Software, Writing – original draft. **Lei Hu:** Software, Formal analysis, Investigation. **Weidong Zhu:** Supervision, Conceptualization, Methodology, Writing – review & editing. **Haolin Li:** Methodology, Validation, Visualization, Project administration.

### **Declaration of Competing Interest**

The authors have no conflict of interest.

### Data availability

Data will be made available on request.

### Acknowledgments

The authors would like to thank the support from the National Science Foundation (Award No. 2117732) and Shanghai Natural Science Foundation (Award No. 21ZR1444000).

# **Appendix A: Fitted Parameters of Temperature Fields**

Fitted parameters of temperature fields as shown in Eq. (2), which are induced by 200 random heating positions, are listed in Table A1.

### Appendix B: Governing Equation of the Plate at High Temperature

A coupled thermal dynamic governing equation of the titanium plate under a non-uniform temperature field can be derived via Hamilton's principle. Substituting thermally coupled stress-strain constitutive equations in Eqs. 5(a)-(c) and geometrical relations in Eq. (8) into the potential energy H in Eq. (9) yields

$$H = \frac{1}{2} \int \int \int \int \left( \sigma_x \varepsilon_x + \sigma_y \varepsilon_y + \tau_{xy} \gamma_{xy} \right) dV = \frac{1}{2} \left( H_1 + H_2 + H_3 + H_4 \right)$$
(B.1)

where

$$H_{1} = \int \int \int \int \psi(T^{*}) \left[ \left( \frac{\partial^{2} w}{\partial x^{2}} \right)^{2} + \left( \frac{\partial^{2} w}{\partial y^{2}} \right)^{2} \right] z^{2} dV, H_{3} = - \int \int \int \int \frac{1}{2} \xi(T^{*}) \left( 2 \frac{\partial^{2} w}{\partial x \partial y} \right)^{2} z^{2} dV,$$

$$H_{2} = \int \int \int \int 2[\psi(T^{*}) + \xi(T^{*})] \frac{\partial^{2} w}{\partial x^{2}} \frac{\partial^{2} w}{\partial y^{2}} z^{2} dV, H_{4} = - \int \int \int \int \chi(T^{*}) T^{*} \left( \frac{\partial^{2} w}{\partial x^{2}} + \frac{\partial^{2} w}{\partial y^{2}} \right) z dV$$
(B.2)

Variations of  $H_i$  with i = 1, 2, 3, 4 can be obtained as

$$\delta H_{1} = \frac{1}{6}h^{3} \begin{pmatrix} \int \delta\left(\frac{\partial w}{\partial y}\right) \frac{\partial^{2} w}{\partial y^{2}} \psi(T^{*}) - \delta w\left(\frac{\partial}{\partial y}\left(\frac{\partial^{2} w}{\partial y^{2}} \psi(T^{*})\right)\right) dx \\ + \int \delta\left(\frac{\partial w}{\partial x}\right) \frac{\partial^{2} w}{\partial x^{2}} \psi(T^{*}) - \delta w\left(\frac{\partial}{\partial x}\left(\frac{\partial^{2} w}{\partial x^{2}} \psi(T^{*})\right)\right) dy \\ + \int \int \delta w\left(\frac{\partial^{2}}{\partial x^{2}}\left(\frac{\partial^{2} w}{\partial x^{2}} \psi(T^{*})\right) + \frac{\partial^{2}}{\partial y^{2}}\left(\frac{\partial^{2} w}{\partial y^{2}} \psi(T^{*})\right)\right) dx dy \end{pmatrix}$$
(B.3)

 $\delta H_2 =$ 

$$\frac{1}{6}h^{3} \left( \int \delta\left(\frac{\partial w}{\partial y}\right) \frac{\partial^{2} w}{\partial x^{2}} [\psi(T^{*}) + \xi(T^{*})] - \delta w \left(\frac{\partial}{\partial y} \left(\frac{\partial^{2} w}{\partial x^{2}} [\psi(T^{*}) + \xi(T^{*})]\right)\right) dx \right) \\
+ \int \delta\left(\frac{\partial w}{\partial x}\right) \frac{\partial^{2} w}{\partial y^{2}} [\psi(T^{*}) + \xi(T^{*})] - \delta w \left(\frac{\partial}{\partial x} \left(\frac{\partial^{2} w}{\partial y^{2}} [\psi(T^{*}) + \xi(T^{*})]\right)\right) dy \\
+ \int \int \left(\delta w \left(\frac{\partial^{2}}{\partial x^{2}} \left(\frac{\partial^{2} w}{\partial y^{2}} [\psi(T^{*}) + \xi(T^{*})]\right) + \frac{\partial^{2}}{\partial y^{2}} \left(\frac{\partial^{2} w}{\partial x^{2}} [\psi(T^{*}) + \xi(T^{*})]\right)\right) dx dy$$
(B.4)

$$\delta H_{3} = -\frac{1}{3}h^{3} \begin{pmatrix} \int \delta\left(\frac{\partial w}{\partial y}\right) \frac{\partial^{2} w}{\partial x \partial y} \xi(T^{*}) dy - \int \delta w \left(\frac{\partial^{3} w}{\partial x^{2} \partial y} \xi(T^{*}) + \frac{\partial^{2} w}{\partial x \partial y} \frac{\partial \xi(T^{*})}{\partial x}\right) dx \\ + \int \int \delta w \left(\frac{\partial^{2} w}{\partial x \partial y} \xi(T^{*})\right) dx dy \end{pmatrix}$$
(B.5)

and  $\delta H_4 = 0$ . Variation of the kinetic energy  $\delta K$  is

$$\delta K = \iiint_{V} \rho \frac{\partial}{\partial t} (\dot{w} \delta w) dV - \iiint_{V} \rho \ddot{w} \delta w dV$$
(B.6)

Due to arbitrariness of  $\delta w$ , the governing equation of the plate can be obtained from Eq. (9), as shown in Eq. (13). Boundary conditions of the plate can also be obtained, as shown in Table 5.

#### References

- L. Wang, M. Xu, Y.H. Li, Vibration analysis of deploying laminated beams with generalized boundary conditions in hygrothermal environment, Compos. Struct. 207 (2019) 665–676.
- [2] L.F. Vosteen, R.R. McWithey, R.G. Thomson, Effect of transient heating on vibration frequencies of some simple wing structures, 4054, NACA Tech. Note, 1955.
- [3] K.D. Murphy, L.N. Virgin, S.A. Rizzi, The effect of thermal prestress on the free vibration characteristics of clamped rectangular plates: theory and experiment, J. Vib. Acoust. 119 (2) (1997) 813–814.
- [4] H. Chen, L.N. Virgin, Dynamic analysis of modal shifting and mode jumping in thermally buckled plates, J. Sound Vib. 278 (2004) 233-256.
- [5] D.J. Mead, Vibration and buckling of flat free-free plates under non-uniform in-plane thermal stresses, J. Sound Vib. 260 (2003) 141-165.
- [6] B.H. Jeon, H.W. Kang, Y.S. Lee, Free vibration characteristics of rectangular plate under rapid thermal loading, Key Eng. Mater. 478 (2011) 81-86.
- [7] Y. Gao, Y.R. Wang, D.H. Xiao, Experimental investigations of thermal modal parameters for a C/SiC structure under 1600 °C high temperature environment, Measurement 151 (2020), 107094.
- [8] X.Y. Li, K.P. Yu, Vibration and acoustic responses of composite and sandwich panels under thermal environment, Compos. Struct. 131 (2015) 1040-1049.
- [9] A.C. Santos, C.M.Sebastian Silva, J. Lambros, E.A. Patterson, High temperature modal analysis of a non-uniformly heated rectangular plate: Experiments and simulations, J. Sound Vib. 443 (2019) 397–410.
- [10] R.R. McWithey, L.F. Vosteen, Effects of transient heating on the vibration frequencies of a prototype of the X-15 wing, NASA Technical Note 362 (1960).
- [11] H. Cheng, H. Li, W. Zhang, B.R. Liu, Z.Q. Wu, F.J. Kong, Effects of radiation heating on modal characteristics of panel structures, J. Spacecr. Rockets 52 (4) (2015) 1228–1235.
- [12] Y.J. Hu, Z.S. Huang, W.D. Zhu, H.L. Li, A full-field non-contact thermal modal testing technique under ambient excitation, Exp. Tech. 45 (3) (2021) 257–271.
- [13] C.D. Bailey, Vibration of Thermally Stressed Plates with Various Boundary Conditions, AIAA. J. 11 (1) (1973) 14-19.
- [14] D. Mead, Vibration and Buckling of Flat Free-Free Plates under Non-uniform In-plane Thermal Stresses, J. Sound Vib. 260 (2003) 141-165.
- [15] F. Alijani, F. Bakhtiari-Nejad, M. Amabili, Nonlinear vibrations of FGM rectangular plates in thermal environments, Nonlinear Dyn 66 (3) (2011) 251–270.
- [16] A.M. Brown, Temperature-dependent modal test/analysis correlation of X-34 FASTRAC composite rocket nozzle, J. Propul. Power 18 (2) (2000) 284–288.
- [17] Y.H. Bai, K.P. Yu, J. Zhao, R. Zhao, Experimental and simulation investigation of temperature effects on modal characteristics of composite honeycomb structure, Compos. Struct. 201 (2018) 816–827.
- [18] Y. Wang, P.F. Mendez, Isotherm penetration depth under a moving Gaussian surface heat source on a thick substrate, Int. J. Therm. Sci. 172 (2022), 107334.
- [19] T. Li, L. Zhang, C. Chang, et al., A Uniform-Gaussian distributed heat source model for analysis of residual stress field of S355 steel T welding, Adv. Eng. Softw. 126 (2018) 1–8.
- [20] Y.J. Hu, H.T. Zhou, W.D. Zhu, J. Chen, Large deformation analysis of composite spatial curved beams with arbitrary undeformed configurations described by Euler angles with discontinuities and singularities, Comput. Struct. 210 (2018) 122–134.
- [21] Y.J. Hu, F. Liu, W.D. Zhu, J.M. Zhu, Thermally coupled constitutive relations of thermoelastic materials and determination of their material constants based on digital image correlation with a laser engraved speckle pattern, Mech. Mater. 121 (2018) 10–20.
- [22] Y.J. Hu, Y.J. Wang, J.B. Chen, J.M. Zhu, A new method of creating high-temperature speckle patterns and its application in the determination of the high-temperature mechanical properties of metals, Exp. Tech. 42 (2018) 523–532.
- [23] C.W. Bert, M. Malik, Differential quadrature method in computational mechanics: a review, Appl. Mech. Rev. 49 (1) (1996) 1-28.
- [24] D.F. Wu, Y.W. Wang, L. Shang, H. Wang, Y. Pu, Experimental and computational investigations of thermal modal parameters for a plate-structure under 1200°C high temperature environment, Measurement 94 (2016) 80–91.
- [25] M. Tsagris, C. Beneki, H. Hassani, On the folded normal distribution, Mathematics 2 (1) (2014) 12, 12.
- [26] J. Liu, Y. Wu, L. Tan, An improvement to the resampling procedure of Bootstrap Method (in Chinese), Mathematical Theory and Applications 26 (2) (2006) 69–72.